JACS
JOURNAL OF THE AMERICAN CHEMICAL SOCIETY
pubs.acs.org/JACS
Article

Wall Teichoic Acids Are Direct Molecular Targets of Antimicrobial Peptides in Gram-Positive Bacteria

Arunima Sandeep, Laila Zaatouf, Alexandre A. Arnold, Dror E. Warschawski, and Isabelle Marcotte*

Cite This: J. Am. Chem. Soc. 2026, 148, 7240−7250
Read Online
ACCESS | Metrics & More | Article Recommendations | Supporting Information

ABSTRACT: Lytic antimicrobial peptides (AMPs) are long recognized for their ability to disrupt bacterial membranes, yet their interactions with other cell-envelope components remain poorly understood. Such knowledge is essential for redesigning AMPs as next-generation antibiotics or tailoring them for strain-specific activity. Here we show, using solid-state and solution NMR, that cationic AMPs engage directly with wall teichoic acids (WTAs)—anionic polymers in the Gram-positive bacteria cell wall. Three representative AMPs acting through different mode of membrane disruption display distinct binding to WTA phosphate groups. Solution NMR of purified WTAs further reveals peptide polymer interactions as well as the residues responsible for recognition. These findings broaden the classical view of AMP action beyond membrane permeabilization, highlighting WTAs as key molecular targets and paving the way for the rational design of peptide antibiotics with tailored specificity.

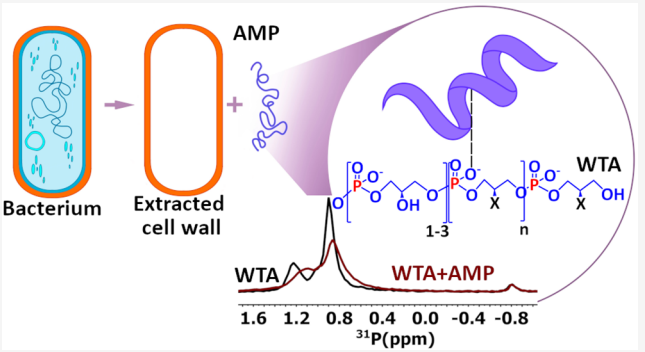

INTRODUCTION

Antimicrobial resistance has become one of the most pressing challenges to human health, prompting the search for alternatives to traditional antibiotics. Antimicrobial peptides (AMPs), also called host defense peptides, are a promising source of inspiration. These short molecules (<50 residues) are integral to the innate immunity of nearly all living organisms and display broad-spectrum activity against bacteria, fungi, viruses, and even tumor cells.[1,2] Research over four decades has shown that many cationic antimicrobial peptides (cAMPs) act through nonspecific interactions with the negatively charged bacterial membranes, including multidrug-resistant strains.[3] Their action mechanism involves membrane micellization or pore formation, which makes the emergence of bacterial resistance difficult.[4,5] Two main factors govern these interactions: the peptide-to-lipid molar ratio (P:L) and the peptide conformational changes, which depend on pH, temperature, and other environmental conditions.[6,7] In aqueous solution, AMPs are largely unstructured but can form structures in membranes or membrane-simulated environments.[2] However, the molecular basis of AMP activity in whole bacteria remains poorly understood, particularly regarding how they engage cell-envelope components beyond phospholipid membranes—a question we address here using solid-state nuclear magnetic resonance (ssNMR) on Gram-positive cell walls.

A substantial proportion of studies on AMPs relied on model lipid systems and were only recently extended to whole cells such as *Escherichia coli*, *Bacillus subtilis* and red blood cell (RBC) ghosts.[8−13] However, a major discrepancy exists between the P:L ratio that perturbs model bacterial membranes (∼1:200), and the much higher ratio required to disrupt intact bacterial membranes (∼10−100:1), as shown for the AMPs omiganan and melittin.[14,15] Our previous ^{2}H ssNMR study of aurein 1.2 and caerin 1.1 with membrane-deuterated bacteria also revealed differences in peptide concentrations that induced phospholipid-chain disorder in Gram(−) *E. coli* vs Gram(+) *B. subtilis*.[16] One explanation for this discrepancy is that AMPs interact with the non-membrane component of the bacterial cell envelope such as lipopolysaccharides, peptidoglycan (PGN), teichoic acids (TAs), or membrane proteins.[16] Electrostatic attraction to the net negative charge of the cell wall may promote peptide accumulation, enabling subsequent membrane damage.[17] Furthermore, the realization that recently discovered antibiotics like teixobactin, clovibactin and hypeptin act by blocking PGN synthesis and compromise membrane integrity, has renewed interest in the bacterial envelope as a chemically diverse and functionally critical target.[18]

Received: October 27, 2025
Revised: January 21, 2026
Accepted: January 26, 2026
Published: February 10, 2026

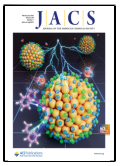

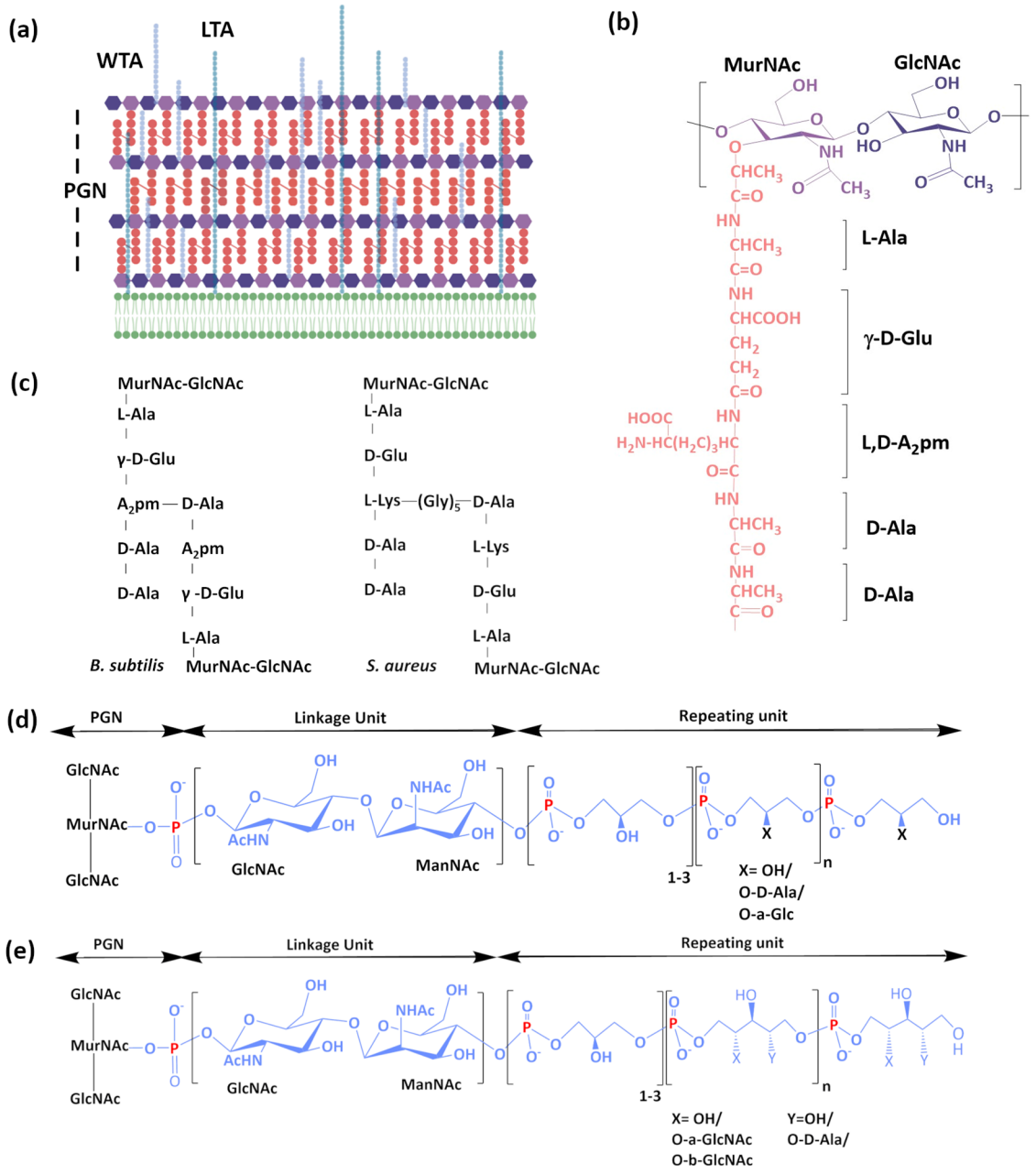

Figure 1. Structure of Gram(+) cell wall components. (a) Schematic of the Gram(+) bacterial envelope showing peptidoglycan (PGN), wall teichoic acids (WTAs), and lipoteichoic acids (LTAs). MurNAc carbohydrates are shown as light purple hexagons, GlcNAc as the dark purple hexagons and the peptide bridge is in pink. (b) Chemical structure of the PGN disaccharide-peptide monomer. (c) Example of interstrand cross-linking in PGN. (d) Structure of *B.* WTA. (e) Structure of *S. aureus* WTA. Phosphate groups are highlighted in red; carbohydrates, glycerol and ribitol backbones of WTA are shown in blue.

To elucidate how cAMPs act at a molecular level and to bridge the gap between model and whole-cell studies, we investigated three amphibian-derived AMPs with distinct action mechanisms and bacterial specificities. Aurein 1.2 (GLFDIIKKIAESF-NH_2, also called aurein) is a short peptide (13 amino acid residues, net charge +1 at pH 7), while caerin 1.1 (GLLSVLGSVAKHVLPHVVPVIAEHL-NH_2, also called caerin) and dermaseptin DMS-DA6-NH_2(GVWGIAKIAGKVLGNILPHVFSSNQS-NH_2, also called DA6) are longer (25 and 26 residues) with net charges of +1 and +3, respectively.[19,20] Their hydrophobicity decreases in the order caerin > aurein > DA6. Previous studies revealed a carpet mechanism for aurein and a pore-forming mechanism for caerin and DA6.[16,21−23] The three AMPs are also known to have more activity toward Gram(+) bacteria.[20,24]

To gain a deeper understanding of how cAMPs engage Gram(+) cell-wall components, we studied their interaction with *B. subtilis* and, in part, with the pathogenic strain *Staphylococcus aureus*. The minimum inhibitory concentrations (MICs) of the three peptides against the two strains were determined to evaluate their antibacterial efficacy. Against *B. subtilis*, the average MICs were 9 μM for aurein, 5 μM for caerin, and 3 μM for DA6. Against *S. aureus*, the average MICs were 34 μM for aurein, 10 μM for caerin, and 2 μM for DA6. Aurein and caerin have a stronger efficacy for *B. subtilis* while DA6 is 1.5 times more efficient on *S. aureus*.[23]

https://doi.org/10.1021/jacs.5c18971
J. Am. Chem. Soc. 2026, 148, 7240−7250

The cell walls of both bacteria (Figure 1a) consist primarily of the disaccharide polymer PGN, composed of N-acetyl glucosamine (GlcNAc) and N-acetyl muramic acid (MurNAc), connected to a stem peptide. The monomer unit of the PGN framework and the stem peptide cross-links in *B. subtilis* and *S. aureus* are shown in Figure 1b,c. The PGN forms an important layer that maintains bacterial shape and resists internal turgor pressure.[25,26] In addition, the negatively charged TAs are covalently linked either to the PGN (wall teichoic acid, WTAs) or to membrane phospholipids (lipoteichoic acids, LTAs).

We utilized ^{13}C and ^{31}P ssNMR on intact cell wall extracts, with and without the cAMPs. ^{13}C ssNMR offers high spectral dispersion that proves to be especially useful when studying carbohydrates, while ^{31}P provides direct access to phosphate groups. The nondestructive nature and atomic resolution of ssNMR, together with multidimensional correlation experiments on isotopically enriched cell-wall material, enabled detailed characterization of these complex AMPs-cell wall systems.

Here, we show that all cationic AMPs preferentially interact with the phosphate and glycan moieties of WTAs in Gram(+) cell walls. Using ^{13}C and ^{31}P ssNMR, complemented by turbidity assays, circular dichroism, and solution NMR, we demonstrate that these interactions modulate WTA dynamics, promote cell-wall aggregation, and, in the case of aurein, induce partial α-helix formation. Residue-level mapping further identifies specific side chains involved in WTA binding, indicating that AMP activity extends beyond membranes to include direct recognition of teichoic acids.

MATERIALS AND METHODS

Materials

The peptides aurein 1.2 and caerin 1.1 were synthesized by GenScript Corporation (Piscataway Township, NJ, USA). DMS-DA6-NH_2 was synthesized by the protein engineering facility of Institut de Biologie Paris-Seine (Sorbonne Université, Paris, France). Peptides are purified as trifluoroacetate salts, with >95% purity, based on HPLC and mass spectrometry. $^{13}C_6$-glucose, sodium dodecyl sulfate (SDS) and the enzymes amylase, DNase, RNase and trypsin were purchased from Sigma-Aldrich. Deionized 18.2 MΩ.cm Milli-Q water was used in all experiments (Millipore-Sigma, Oakville, ON, Canada).

Cell Growth

Bacillus subtilis PY79 strains and *S. aureus* (ATCC 6538) were used in the study. *B. subtilis* was kindly provided by Prof. Éric Déziel (Institut Armand-Frappier, Laval, Québec, Canada). Cells were grown in nutrient-rich Luria−Bertani (LB) medium buffered with NaOH to pH 7.4. Bacterial cultures were grown at 37 °C with orbital agitation at 220 rpm. The early stationary phase (optical density (OD) between 2 and 3) in a 300 mL culture was reached after 6 h, with cells inoculated at an initial OD of 0.1. Bacteria were harvested by centrifugation at 3000*g* for 10 min after reaching the early stationary phase. The protocol used for measuring the MIC of *B. subtilis* and *S. aureus* is in the Supporting Information (Protocol S1).

^{13}C Isotopic Labeling

An M9 minimal medium supplemented with 0.9 g of fully ^{13}C-labeled glucose per 300 mL was utilized with both bacterial strains. Detailed content and preparation of the medium are described in the Supporting Information (Protocol S2 and Table S6−8). The early stationary phase was reached after approximately 16 h of growth started at an OD of 0.1.

Cell Wall Extraction

The cell wall was extracted using a modified protocol from Bui et al.[27] detailed in the SI (Protocol S3). Briefly, cell pellets were rinsed twice with a 0.85% NaCl solution and then freeze-dried. Then, the dried pellets were treated with a 1% SDS solution and boiled for 30 min to break the lipid membrane and release the cell content. Cell wall elements were recovered by centrifuging at 4000*g* for 15 min. Treatment with amylase, DNase, RNase and trypsin was performed to remove unwanted proteins and nucleic acids from the cell wall. The protocol yields a purified cell wall, called sacculi, that retains the shape of the bacteria from which it was extracted, as shown in Figure S1a.

Wall Teichoic Acid Extraction

A well-established alkaline hydrolysis protocol was utilized, and extract purity was assessed by ^{1}H and ^{31}P NMR (see ains the shape of the bacteria Figure S1a). The previously extracted cell wall was treated with 0.1 M NaOH for 16 h at room temperature with 220 rpm shaking to remove the WTAs. Centrifugation at 5500*g* for 45 min was performed to obtain the WTA-containing supernatant, which was then precipitated with three volumes of 95% ice-cold ethanol and 0.1 volume of 3 M sodium acetate (pH 5.1). After an overnight precipitation, a second centrifugation at 5500*g* for 30 min yielded the WTA pellet, which was resuspended in nanopure water and lyophilized for storage at −20 °C.[28]

Nuclear Magnetic Resonance

All NMR experiments were performed on a solution/solid-state hybrid 600 MHz Bruker Avance III HD spectrometer (Milton, Ontario, Canada). For ssNMR experiments, samples were prepared by incubating 5 mg of cAMP with 10 mg of freeze-dried cell wall rehydrated in 200 μL D_2O (pH 6−7), a mass ratio (cAMP: cell wall) determined independently by an absorbance experiment with the DA6 peptide, as explained in the SI (Figure S1b). The mixture was agitated at room temperature for 1 h, centrifuged and packed into a rotor to achieve a hydrated sample weight of 35−40 mg. Experiments were carried at 15 °C with a Varian BioMAS 3.2 mm triple resonance HXY probe, using 15 kHz magic angle spinning (MAS) to prevent rotational resonance and spinning sideband interference. Cross-polarization (CP) with a 1.5 ms contact time was applied to detect rigid components, whereas refocused INEPT (Insensitive Nuclei Enhanced by Polarization Transfer) experiments (two 1.78 ms delays followed by two 890 μs delays) were used for mobile species. To assign glycan and amino acid resonances, a 2D ^{13}C refocused NOE-INADEQUATE (Nuclear Overhauser Effect-Incredible Natural Abundance DoublE QUAntum Transfer Experiment) spectrum was recorded initiated with a 2 s ^{1}H to ^{13}C NOE.[29] A 1 s recycle delay and 64 scans were used. The spectral width was set to 90 kHz along F1 and 45 kHz along F2. Resonance assignments are summarized and compared with literature values in Supporting Tables S1−S2.[30,31] Spin−lattice relaxation times (T_1) were measured by inversion recovery, and transverse relaxation times (T_2) by the Hahn echo experiment for both ^{31}P and ^{13}C nuclei. Relaxation data were fitted using a single-exponential decay function.

For solution NMR, samples were prepared in 80% H_20 and 20% D_2O. All three peptides were mixed with WTAs at identical molar ratios of cAMPs: WTA. The approximate molecular mass of WTA was estimated by assuming a repeating polymer of 40 units with 13 of the units to be substituted with glucose, 13 units to be with D-alanine and the remaining unsubstituted, yielding a molecular mass of 11 kDa. The approximate WTA concentration used in the experiments was 9 μM, while peptide concentrations ranged from 274 to 110 μM. The cAMP:WTA ratios chosen for solution NMR experiments were 30:1, 15:1, and 12:1. These are approximate molar ratios determined by an approximate molecular weight of WTA, so all molar ratios referred to henceforth are approximate. Experiments were performed at 23 °C using a 5 mm BBFO probe. $^{1}H-^{1}H$ TOCSY (TOtal Correlation SpectroscopY) experiments with an 80 ms contact time, during which a MLEV spin-lock pulse at an RF power of 10 kHz was applied to examine the effect of WTA on the amino-acid residues of the peptides. Peptide NMR signal assignments were performed using a stepwise approach, starting in the amide (NH) region and utilizing TOCSY correlations to the H_α, H_β, and other protons. Residues with distinctive chemical shifts, such as phenylalanine, were assigned first, followed by more crowded regions containing leucine, isoleucine, and valine residues. Average chemical shifts from the Biological Magnetic

https://doi.org/10.1021/jacs.5c18971
J. Am. Chem. Soc. 2026, 148, 7240−7250

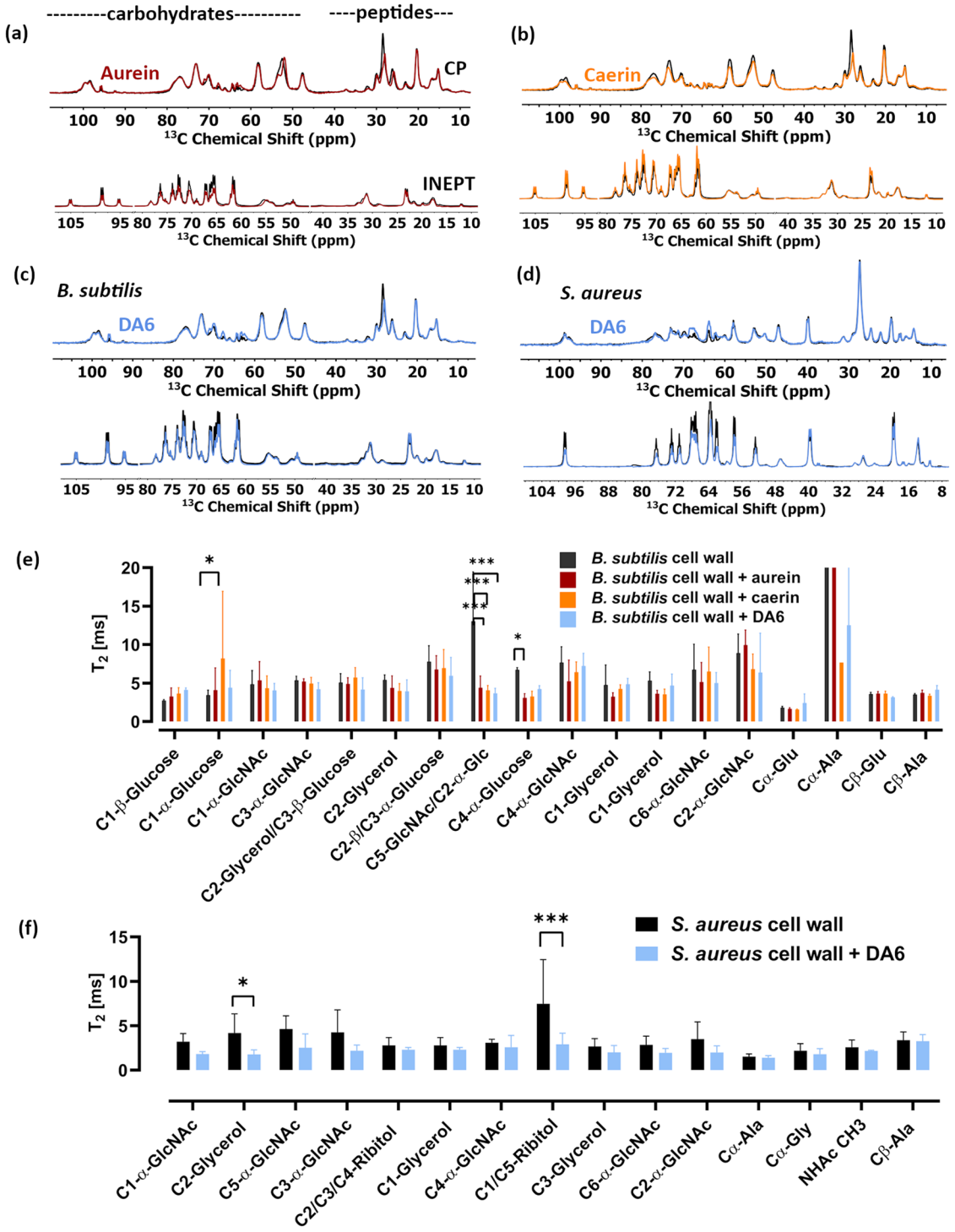

Figure 2. ^{13}C ssNMR and T_2 relaxation measurements on cell wall extracts. 1D ^{13}C CP (top) and INEPT (bottom) spectra of carbohydrates and stem peptides in the *B. subtilis* cell wall extracts recorded before (black) and after incubation with (a) aurein (red), (b) caerin (orange), and (c) DA6 (blue) as well as (d) *S. aureus* cell wall extracts (black) with DA6 (blue). Panels (e) and (f) show the averaged ^{13}C T_2 measurements of cell wall extracts from *B. subtilis* and *S. aureus* before and after incubation with the cAMPs, respectively. Bars represent the mean of three independent experiments, with error bars indicating the standard deviation.

Resonance Data Bank (BMRB) guided the assignment process. When ambiguities arose in the TOCSY spectra, NOESY (Nuclear Overhauser Effect SpectroscopY) spectra were used to resolve overlapping signals and confirm sequential connectivities.

Optical Microscopy

ssNMR samples were stained with crystal violet dye according to the Gram staining protocol. Before staining, samples were resuspended in 500 μL methanol, then 20 μL of this suspension was placed on a slide, gently heated at 40 °C to dry and fix the material. Images were acquired using a Nikon Ti inverted microscope with a 20× objective.

Turbidity

To assess sample turbidity, a series of cAMP:WTA molarity ratios were prepared. The mixtures were transferred to semi-micro1.5 mL cuvettes (Fisher Scientific), and turbidity was measured at 600 nm

https://doi.org/10.1021/jacs.5c18971
J. Am. Chem. Soc. 2026, 148, 7240−7250

using a Biochrome Libra Visible S6+ spectrophotometer (Montréal, Québec, Canada).

Circular Dichroism

Samples were prepared at cAMP:WTA molar ratios of 15:1, 12:1, 6:1, and 3:1 using nanopure water, at pH 6−7. A 0.2 cm path length quartz cell was employed. For the KCl test, WTA was first mixed with 50 mM KCl to block the charged phosphates, before adding the peptides at a selected 6:1 cAMP:WTA molar ratio. Far-UV CD spectra were recorded from 190 to 260 mm using a Jasco J-815 CD spectrometer (Easton, MD, USA) with a wavelength step of 0.5 nm and a scanning speed of 20 nm/min. Spectra were background-subtracted using peptide-free water and further corrected by subtracting the WTA control spectrum. Raw data were converted to mean residue ellipticity (MRE), and spectral deconvolution was performed with Dichroweb (a Website for calculating protein secondary structure from CD data) using the CDSSTR algorithm and the SMP 180t data set.[32]

Statistical Analysis

Statistical analysis was performed using the 2-way ANOVA multiple comparison test. Significant statistical difference was established as $p < 0.06$ (*), $p < 0.01$ (**) and $p < 0.001$ (***). Graphpad Prism 8.4 software was utilized for the test and for the analysis/plotting of the bar graphs.

RESULTS AND DISCUSSIONS

Antimicrobial Peptides Preferentially Interact with WTAs

We investigated the interactions of aurein, caerin, and DA6 with purified and intact sacculi of *B. subtilis*, which only comprise the PGN and WTAs as shown in Bui et al.[27] First, standard two-dimensional (2D) $^{13}C-^{13}C$ SQ-DQ refocused INADEQUATE experiments allowed us to assign the glycan and glycerol resonances in the ^{13}C-labeled cell walls of both *B. subtilis* and *S. aureus* (Figure S3 and Tables S1−S2). We then screened the interaction sites by 1D ^{13}C ssNMR using CP- and INEPT-based experiments, which respectively probe rigid and flexible components of the cell wall.[33,34] Figures 2a−c, show that the stem peptides within the cell wall are more rigid than carbohydrate moieties, with only minor changes in the CP spectra in the presence of the cAMPs. By contrast, INEPT spectra reveal that aurein and DA6 slightly decrease signal intensity in the carbohydrate region, while caerin produces a modest increase. These results indicate that the cAMPs primarily interact with flexible carbohydrate components rather than the rigid stem peptides within the peptidoglycan framework.

Using DA6 we performed the same experiments on the more pathogenic Gram(+) bacterium *S. aureus*, given that DA6 has demonstrated activity against this strain and represents a promising candidate for treating *S. aureus* infections.[20,23] The structure of its cell wall differs from that of *B. subtilis*, with the PGN cross-links formed by a pentaglycine bridge. The WTAs are mainly composed of ribitol phosphate units, in contrast to the glycerol phosphate backbone characteristic of *B. subtilis*. The positions and types of substituents also vary: in *B. subtilis*, D-Ala or glucose are attached at the C2 position of glycerol phosphate, whereas in *S. aureus*, substitutions occur at both C2 and C4 of ribitol with either GlcNAc, D-Ala, or both (See Figure 1d,e). The number and distribution of WTA substitutions in both organisms are variable and can depend on growth conditions.[35] Different results were obtained for DA6 in *S. aureus* compared with *B. subtilis*. The 1D ^{13}C INEPT experiment revealed that DA6 induces a slight increase in signal intensity in the carbohydrate moieties of the *S. aureus* cell wall, whereas the corresponding ^{13}C CP spectrum shows a decrease in the same region. This result is likely a consequence of a marginal enhancement of carbohydrate mobility which would reduce cross-polarization—efficient for rigid sections—while increasing the through-bond INEPT transfer which is most effective for mobile segments. As in *B. subtilis*, the stem peptides in the cell wall of *S. aureus* showed almost no detectable effects in the peak intensities.

We thus measured the ^{13}C T_1 and T_2 relaxation times to confirm dynamic changes in the cell wall in the presence of the cAMPs.[36] Different NMR relaxation times provide information on dynamical processes occurring at distinct time scales. T_1 is sensitive to fast local motions, typically on the nanosecond time scale, whereas T_2 is sensitive to slower motions, on the order of milliseconds or less. If fast local motions (e.g., methyl rotations) remain unchanged upon peptide addition, then T_1 is unaffected (Figure S4a,b). In contrast, reductions in collective motion, such as aggregation, which occur on slower time scales, can be observed as a change in T_2. Indeed, significant alterations were observed in T_2 values: in *B. subtilis*, all cAMPs consistently affected the glucose carbons of the WTAs (Figure 2e), while in *S. aureus*, DA6 produced clear effects at the C2 position of glycerol and the C1/C5 of the ribitol moiety (Figure 2f). A comparable trend has been reported for highly charged cationic nanoparticles, which preferentially interact with WTA glycerol backbones and attached glucose residues.[37]

These results suggest that the cAMPs preferentially interact with the WTAs of the cell wall, warranting further investigation. Because WTAs contain phosphorus atoms, we acquired and assigned 1D ^{31}P ssNMR spectra of the bacterial sacculi. Three distinct peaks in the ^{31}P ssNMR of the extracted cell wall were assigned, as shown in Figure 3a. From left to right, the first peak corresponds to unsubstituted glycerol phosphates in the WTAs, the second to glycerol phosphates substituted with D-Ala or glucose, and the third peak to the phosphate linking WTAs to the PGN, hereafter referred to as the linker (see Figure 1d,e).[30,37] In the presence of cAMPs, peak broadening is observed for both bacterial strains, except for the linker phosphates, which are structurally embedded within the PGN (Figure 3a,b).

This broadening likely reflects increased structural disorder or dynamic changes affecting the phosphate moieties.[29] Notably, the proportion of substituted phosphates exceeds that of unsubstituted phosphates in *B. subtilis* and vice versa for *S. aureus* (Figure 3b). This observation could be correlated with the differences in the ^{13}C T_2, as the lower degree of substitution in *S. aureus* leaves the WTA backbone chains, such as ribitol, more accessible for peptide binding.

To investigate dynamic changes near the phosphorus atoms in the WTAs induced by cAMP interactions, we measured ^{31}P T_1 and T_2 relaxation times. As observed based on the ^{13}C T_1 measurements, fast molecular motions with frequencies on the order of MHz showed little variation upon addition of the cAMPs (Figure S4c,d). In contrast, T_2 values were significantly altered by all three peptides, with statistical analysis indicating the following order of effect: aurein > caerin > DA6 (Figure 3c), corresponding to an average decrease of 80% (with aurein) and 70%(with caerin) for the unsubstituted phosphates. For the substituted phosphates, the percentage of decreases are 76% and 65% for aurein and caerin, respectively. Note that for DA6, the average change falls within experimental error. Consistent with the 1D ^{31}P ssNMR

https://doi.org/10.1021/jacs.5c18971
J. Am. Chem. Soc. 2026, 148, 7240−7250

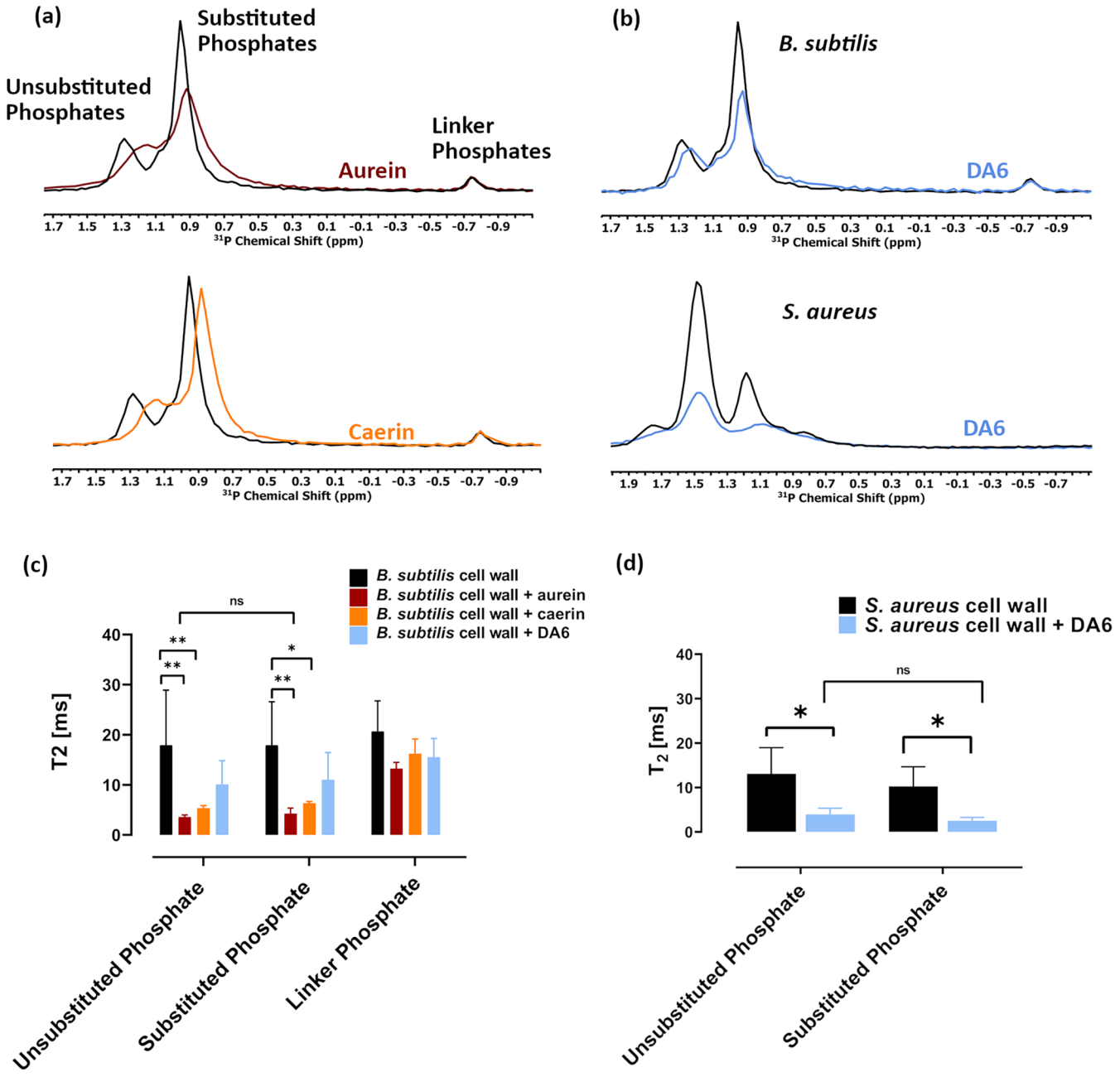

Figure 3. ^{31}P ssNMR and T_2 relaxation measurements on cell wall extracts.^{31}P ssNMR spectra of extracted cell walls (a) from *B. subtilis* in the absence (black) and presence of aurein 1.2 (red) or caerin 1.1 (orange), and (b) from *B. subtilis* (black) and *S. aureus* (black) without or with DA6 (blue), along with the effect of AMPs on the T_2 values of the ^{31}P resonances in (c) *B. subtilis* and (d) *S. aureus*. Bars represent the mean of three independent experiments, with error bars indicating the standard deviation. No significant differences were detected between substituted and unsubstituted phosphates.

experiments, T_2 measurements also confirmed the absence of dynamic alterations in the linker phosphates.

These experiments indicate that all cAMPs examined in this study preferentially interact with the substituted and unsubstituted phosphates, as well as glycan/glycerol-ribitol moieties of the WTAs as revealed by ^{13}C experiments. By contrast, no significant dynamic changes or interactions were observed with the PGN. Because DA6 interacts with the WTAs of both *B. subtilis* and *S. aureus*, these findings emphasize the general ability of cAMPs to bind TAs in Gram(+) bacteria (Figure 3d). Comparing the effect of DA6 on the two strains, we observed a statistically significant decrease in the ^{31}P T_2 value only for *S. aureus*, in both substituted (75%) and unsubstituted phosphates (70%), indicating a stronger interaction with this strain. The difference in DA6 binding between *S. aureus* and *B. subtilis* may be influenced by their underlying PGN architecture. The length of the peptide bridge is a major determinant of cell wall organization: the pentaglycine bridge in *S. aureus* supports a tightly packed, parallel-stem architecture, while *B. subtilis*, which lacks a bridge, adopts a more open antiparallel arrangement with lower cross-linking density.[38] These structural differences are likely to affect the accessibility of WTAs to the AMPs. Altogether, these results suggest that all

https://doi.org/10.1021/jacs.5c18971
J. Am. Chem. Soc. 2026, 148, 7240−7250

three cAMPs, with different action mechanisms and chemical characteristics, are located in the vicinity of the glycerol/ribitol phosphates of the WTAs.

Antimicrobial Peptides Induce Aggregation and Can Undergo Conformational Changes in the Presence of WTAs

The significant interaction with WTAs revealed by ^{13}C and ^{31}P ssNMR prompted us to examine (1) whether this interaction induces effects observable at the mesoscopic scale, (2) whether the cAMPs undergo conformational changes, and (3) which specific regions of their sequences are involved in the interaction. Interestingly, in the presence of cAMPs, we observed aggregation of the whole purified sacculi (containing both PGN and WTAs) by optical microscopy following Gram staining (Figure 4a–d and S5a,b) after the ^{31}P 1D ssNMR

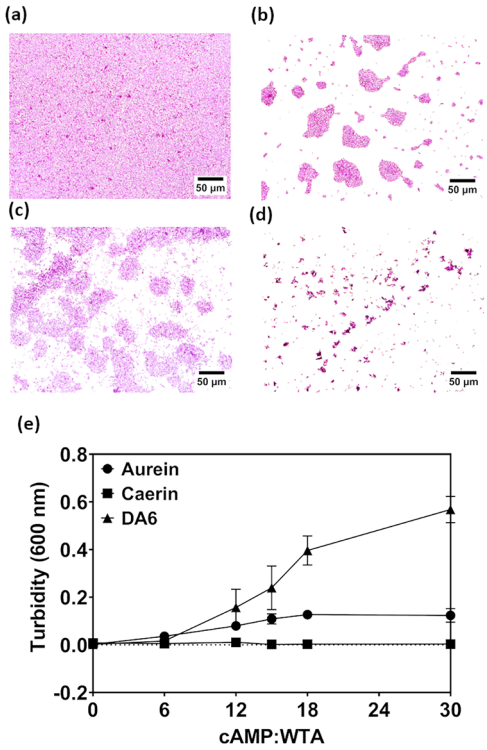

Figure 4. Microscopy and turbidity studies of cAMP interactions with *B. subtilis* cell wall and WTA. Optical microscopy images of (a) *B. subtilis* cell wall with (b) aurein, (c) caerin, and (d) DA6. All samples are collected after the ^{31}P ssNMR experiments. The scale bar represents 50 μm. (e) Turbidity measurements of *B. subtilis* WTA and cAMPs determined by visible spectrophotometry at 600 nm at various peptide-to-WTA molar ratios.

experiments. The extent of aggregation varied among peptides: DA6 produced relatively small aggregates, whereas aurein and caerin formed larger aggregates. This observation is consistent with the reduction in T_2 values, which indicate slower molecular motions, likely arising from aggregation. While the aggregation effect is clear, we cannot ascertain changes at the molecular scale. However, given the rigidity of these structures, thinning or swelling, for example, is unlikely.

To further demonstrate the preferential interaction of the cAMPs with the WTAs, we isolated these components from the cell wall and performed turbidity measurements. The cAMP-WTA interaction proved to be strong enough to be detected macroscopically. Varying the cAMP:WTA approximate molar ratio produced changes in turbidity at 600 nm (Figure 4e) and, in some cases, led to precipitation. As the concentrations of aurein and DA6 increased, the turbidity of the samples also increased until reaching a plateau, whereas the samples containing caerin remained transparent. This observation correlates with peptide hydrophobicity: the least hydrophobic peptide, DA6 (GRAVY = 0.465), produced the highest turbidity, while the most hydrophobic, caerin (GRAVY = 1.143), produced the lowest; aurein showed intermediate behavior (GRAVY = 0.669). The trend suggests that peptide hydrophilicity modulates the extent of peptide-WTA aggregation.

The turbidity experiment enabled us to establish the boundaries for investigating the cAMP-WTA interaction in solution using analytical techniques such as circular dichroism (CD) and solution NMR. We found a maximum WTA concentration of 0.1 mg/mL above which precipitation occurs, and a maximum cAMP:WTA (30:1) molar ratio beyond which samples precipitate (Figure 4). Within these limits, the peptides can interact with the WTAs while remaining in solution long enough for CD and overnight solution NMR experiments. It should be noted that for solution-state NMR there is a minimum cAMP:WTA (6:1) ratio at which the interaction takes place but falls below the detection limit of the technique in our conditions.

Given the binding of cAMPs to WTAs, we next assessed whether the transition from aqueous solution to the WTA environment induces structural changes in the peptides. At cAMP:WTA ratios of 15:1 or lower, CD analysis showed that aurein adopts an α-helical conformation in the presence of WTAs, as shown in Figure 5a. By contrast, no detectable structuring was observed for caerin and only minor changes for DA6, at the lowest concentrations (Figures S6 and S7a). To assess whether the cAMP-WTA interaction is electrostatic in nature, we added varying concentrations of KCl to cAMP:WTA samples at fixed molar ratios of 6:1. The CD spectra showed that 50 mM KCl (Figure S7b) inhibited the α-helical structuring of both aurein and DA6, supporting the electrostatic origin of the interaction.

To identify the interaction sites on the cAMPs, we monitored their chemical shift changes when interacting with WTA, using solution ^{1}H NMR. The maximum usable WTA concentration was limited by sample aggregation, which otherwise prevented detection of cAMP signals. By maintaining the concentration limit and ratios determined by turbidity experiments, we observed that the chemical shifts of the N–H region of specific amino acids shifted upfield or downfield as WTA concentration increased in the ^{1}H–^{1}H TOCSY spectra. Several amino acid residues were affected in aurein with changes ranging from 0.03 up to 0.3 ppm for Asp4 NH (Figure 5b). For caerin, the most significant changes were observed with Leu14, His16, His24, and especially Glu23 (Figure S8a). We also examined the effect of WTA on DA6 (Figure S8b), where four residues were perturbed, the largest shift being observed for Asn15. The chemical-shift changes of all the residues in all three cAMPs are depicted in Figure 5c, with complete data provided in Tables S3–S5. A shift difference of $\geq$ 0.04 ppm was arbitrarily taken as significant.

Although several charged residues were affected in each cAMP, no consistent pattern emerged, and mapping equivalent residues across peptides was not possible. Overall, NH protons were the most affected, with smaller changes detected in Hα and Hβ signals. The ^{1}H NMR results likely reflect local

https://doi.org/10.1021/jacs.5c18971
J. Am. Chem. Soc. 2026, 148, 7240–7250

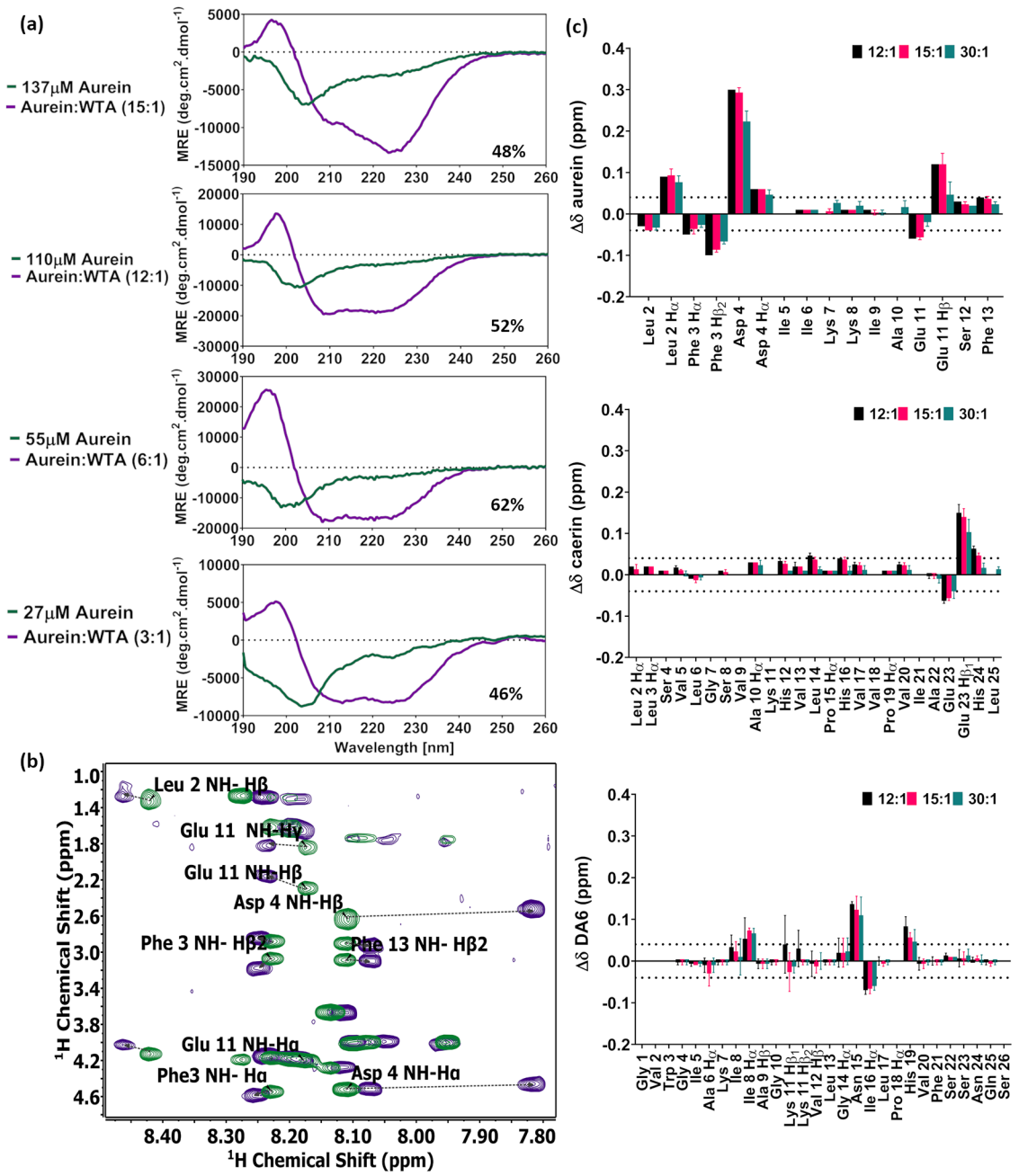

Figure 5. Conformational and chemical shift changes of cAMPs in the presence of *B. subtilis* WTA. (a) CD spectra of extracted *B. subtilis* WTA at different aurein:WTA molar ratios. The helicity value for aurein is indicated in the figure. (b) Overlayed $^{1}H-^{1}H$ TOCSY spectrum of the amide aliphatic region of aurein alone (green) and with WTA at a 15:1 molar ratio (purple). The amino acids affected by the presence of WTA are highlighted with the dotted line showing the chemical shift change. (c) Chemical shift changes of all amino acids when interacting with WTA for the three cAMPs (NH chemical shifts are plotted unless specified). The dotted line shows the arbitrary threshold (≥0.04 ppm) chosen for determining the perturbed residues. Bars represent the mean of three independent experiments, with error bars indicating the standard deviation.

structural changes or changes in H-bonding - possibly due to aggregation that reduces solvent accessibility—arising from an interplay between electrostatic and hydrophobic interactions. The magnitude of these effects appears to depend on the specific chemical properties of each cAMP, as will be discussed below.

For aurein, we observed a discrepancy between the secondary-structure change detected by CD and the chemical shift analysis by NMR which showed that it was random coil. At the concentration used for NMR (30:1, 15:1 and 12:1), CD indicated approximately 40−50% helicity, with the remaining population likely adopting coil or turn conformations (Figures 5a and S7a). This difference reflects the distinct sensitivities of the two techniques: CD could readily detect partially populated or transient helical conformations, whereas NMR chemical shifts are dominated by the predominant conformer. The disparity is further accentuated by the characteristic time scales of the measurements, with solution NMR probing motions on the tens-of-microseconds time scale, while CD reports on much faster processes, estimated to occur on subpicosecond time scales.[39,40] Collectively, these observations indicate that the interaction between aurein and the WTAs is

https://doi.org/10.1021/jacs.5c18971
J. Am. Chem. Soc. 2026, 148, 7240−7250

likely transient, with the observed chemical shifts representing an average between bound (structured) and free (unstructured) peptide populations.

The interaction of WTAs with the three cAMPs aurein, caerin, and DA6 revealed notable differences in chemical shift perturbations, structural responses, and macroscopic effects such as turbidity changes, all of which may reflect distinct mechanisms of initial cell-wall engagement. Aurein displayed strong interactions with WTAs, evidenced by pronounced chemical-shift changes particularly for Asp14, and concentration-dependent increase in turbidity. In addition, aurein adopted an α-helical conformation indicating that WTA binding promotes structural ordering. These findings support the hypothesis that aurein engages with WTAs in the cell wall prior to membrane disruption, with prestructuring potentially influencing subsequent membrane activity.

By contrast, caerin, characterized by a higher hydrophobicity, longer sequence, and net positive charge, exhibited chemical-shift perturbations localized to Leu14, His16, Gln23, and His24, but induced neither turbidity nor secondary structure formation. These results suggest that at the same molar ratio as aurein, caerin interacts with WTAs more weakly, or in a fundamentally different manner. This behavior is consistent with its proposed pore-forming mechanism, which may require a larger amphipathic interface, such as the cytoplasmic membrane, for stable interaction.

DA6 exhibited an intermediate profile. Although it shares a similar sequence length with caerin and has a higher net positive charge, its lower hydrophobicity distinguishes it. Four residues displayed chemical-shift perturbations, with Asn15 the most affected. Turbidity increased in a manner similar to aurein, suggesting aggregation or complex formation with WTAs. However, DA6 underwent only modest structural changes, observed at lower concentrations in CD experiments. This behavior suggests a less ordered binding mode that does not necessarily involve substantial conformational adaptation.

Altogether, these observations indicate that structural adaptability upon WTA binding may contribute to the mechanism of action for shorter cAMPs like aurein, whereas larger, pore-forming peptides such as caerin and DA6 may interact only weakly or transiently with cell-wall components, preferring the membrane as the principal site of structural engagement. It is noteworthy that the structurally related lipoteichoic acids are likely to engage similar interactions with these peptides. However, because our extracts are devoid of lipoteichoic acids, such interactions could not be assessed here and remain to be established.

An important question remains whether such interactions with WTAs favor or hinder antimicrobial activity. Teichoic acids are anionic polymers, and most AMPs are cationic, making electrostatic attraction likely. Indeed, we demonstrated this electrostatic contribution by screening with KCl. However, comparison of three AMPs with differing net charges showed that electrostatics alone do not account for peptide binding. Instead, a subtle interplay between electrostatic charge, hydrophobicity, and peptide sequence flexibility governs the interaction.

Binding to WTAs may trap AMPs within the cell wall, thereby reducing the effective peptide concentration at the cytoplasmic membrane and diminishing antimicrobial potency.[17] Consistent with this hypothesis, isolated lipoteichoic acids reduce the activity of PBP 10, LL-37 and melittin.[41] Our results extend this observation to intact cell walls, suggesting that such an effect may be general among cAMPs. Along these lines, it is interesting to note that aurein, which shows stronger interaction with WTAs, also has the highest MIC against *B. subtilis*.

Conversely, other studies have proposed that WTA binding may facilitate AMP access to the membrane by serving as a polyanionic ladder for polycationic molecules.[42] For example, *S. aureus* TagO mutants lacking WTAs exhibit increased resistance to both human β-defensin and mammalian group IIA phospholipase A_2.[43] In Gram-negative bacteria, the interaction of cationic peptides with lipopolysaccharides has been proposed to indirectly perturb the membrane, thus enhancing peptide uptake into the cell.[44,45] For membrane-perturbing peptides such as those considered herein, such an indirect weakening of the membrane could facilitate its disruption through carpet or pore-forming mechanisms. Integrating our results into this model suggests a multistep process preceding final membrane disruption: (i) an initial electrostatic capturing of the peptide by cell-wall components, in some cases accompanied by prestructuring of the peptide; (ii) a subsequent weakening of the membrane barrier; and (iii) enhanced peptide access to the membrane, ultimately enabling pore formation or micellization. In light of our results, a self-promoting interaction cannot be proven but cannot be ruled out. It is tempting to ascribe the lowest potency of caerin compared to DA6 to its stronger interaction with WTAs; however, the lower MIC of DA6 and transient interactions with the cell wall reflect a self-promoting mechanism.

Overall, this study revealed that AMP activity extends beyond membrane permeabilization, implicating WTAs as important molecular targets. Future studies will be required to refine our understanding of membrane-active AMP mechanisms, taking into account the mode of peptide interaction with the membrane (carpet versus pore-forming) and the relative affinity of the peptide for the membrane versus the cell wall.

CONCLUSION

This work demonstrates the role of the Gram(+) bacterial cell wall in the mechanism of action of cAMPs. Using cell-wall isolates and ssNMR, we showed that representative peptides bind to the cell wall, with WTAs emerging as their principal interaction partners. Our results emphasize the need to account for the cell wall—particularly WTAs—when deciphering cAMP activity against Gram(+) bacteria. A well-established resistance strategy in these bacteria involves increasing D-alanylation of WTAs, which reduces the net negative surface charge and thereby decreases cAMP affinity.[46,47] Our findings support the view that such modifications directly influence both binding and antimicrobial efficacy. By revealing WTAs as key molecular targets, this study provides a framework for understanding how AMP-cell wall interactions shape antimicrobial outcomes. Extending these investigations to intact cells with *in-cell* ssNMR will enable direct observation of peptide-cell wall interactions in their native environment, offering deeper mechanistic insight into the structural and dynamic basis of AMP activity.

ASSOCIATED CONTENT

Supporting Information

The Supporting Information is available free of charge at https://pubs.acs.org/doi/10.1021/jacs.5c18971.

https://doi.org/10.1021/jacs.5c18971
J. Am. Chem. Soc. 2026, 148, 7240−7250

Supporting Information includes optical microscopy of extracted PGN and absorbance spectroscopy with DA6; solution-state ^{1}H and ^{31}P NMR of extracted WTAs; ^{13}C SQ−DQ RINADEQUATE assignments of the carbohydrate and peptide regions; ^{13}C and ^{31}P T_1 relaxation times of *B. subtilis* and *S. aureus* cell walls in the presence of cAMPs; crystal violet−stained cell wall images of *B. subtilis* with cAMPs; conformational analysis of caerin and DA6 in the presence of WTAs; percentage helicity and the effect of KCl on cAMPs; TOCSY spectra of caerin and DA6 with WTAs. Supporting tables provide carbon resonance assignments for the cell walls of *B. subtilis* and *S. aureus*, ^{1}H chemical shift assignments of aurein, caerin, and DA6 with and without WTAs, and detailed media compositions. Supporting protocols describe MIC determination, isotopic labeling of bacteria using M9 media, and extraction of Gram-positive bacterial cell walls. (PDF)

AUTHOR INFORMATION

Corresponding Author

Isabelle Marcotte − *Department of Chemistry, Université du Québec à Montréal,, Montréal, Québec H2X 2J6, Canada;* orcid.org/0000-0001-7467-7119; Email: marcotte.isabelle@uqam.ca

Authors

Arunima Sandeep − *Department of Chemistry, Université du Québec à Montréal,, Montréal, Québec H2X 2J6, Canada*

Laila Zaatouf − *Chimie Physique et Chimie du Vivant, CPCV, CNRS UMR 8228, Sorbonne Université, École Normale Supérieure, PSL Université, 75005 Paris, France*

Alexandre A. Arnold − *Department of Chemistry, Université du Québec à Montréal,, Montréal, Québec H2X 2J6, Canada;* orcid.org/0000-0001-9624-6416

Dror E. Warschawski − *Department of Chemistry, Université du Québec à Montréal,, Montréal, Québec H2X 2J6, Canada; Chimie Physique et Chimie du Vivant, CPCV, CNRS UMR 8228, Sorbonne Université, École Normale Supérieure, PSL Université, 75005 Paris, France;* orcid.org/0000-0002-4363-4965

Complete contact information is available at: https://pubs.acs.org/10.1021/jacs.5c18971

Author Contributions

The manuscript was written through contributions of all authors. All authors have given approval to the final version of the manuscript.

Notes

The authors declare no competing financial interest.

ACKNOWLEDGMENTS

This research was funded by the Natural Sciences and Engineering Research Council (NSERC) of Canada (grant RGPIN-2024-05667 to I.M.), and the Centre National de la Recherche Scientifique (UMR8228 and IEA PamGram + to DEW) and the Agence Nationale de la Recherche (ANTAR-BioTic to DEW). A.S. and L.Z. would respectively like to thank the Fonds de recherche du Québec-Nature et technologies (10.69777/371540) and Sorbonne Université for the award of scholarships. The authors are grateful to Dr. Phuong Trang Nguyen and Dr. Grégoire Bonnamour (Université du Québec à Montréal) for the technical guidance in CD and optical microscopy, respectively. We also thank Dr. François Otis for his help with CD analysis, and Dr. Stéphane Beauclercq for technical support in statistics.

REFERENCES

(1) Naghavian, R.; Faigle, W.; Oldrati, P.; Wang, J.; Toussaint, N. C.; Qiu, Y.; Medici, G.; Wacker, M.; Freudenmann, L. K.; Bontè, P.-E.; et al. Microbial peptides activate tumour-infiltrating lymphocytes in glioblastoma. *Nature* **2023**, *617*, 807−817.

(2) Li, X.; Zuo, S.; Wang, B.; Zhang, K.; Wang, Y. Antimicrobial mechanisms and clinical application prospects of antimicrobial peptides. *Molecules* **2022**, *27*, 2675.

(3) Valenti, G. E.; Alfei, S.; Caviglia, D.; Domenicotti, C.; Marengo, B. Antimicrobial peptides and cationic nanoparticles: a broad-spectrum weapon to fight multi-drug resistance not only in bacteria. *Int. J. Mol. Sci.* **2022**, *23*, No. 6108.

(4) Bechinger, B.; Gorr, S. U. Antimicrobial Peptides: Mechanisms of Action and Resistance. *J. Dent Res.* **2017**, *96*, 254−260.

(5) Peschel, A.; Sahl, H.-G. The co-evolution of host cationic antimicrobial peptides and microbial resistance. *Nat. Rev. Microbiol.* **2006**, *4*, 529−536.

(6) Sani, M.-A.; Separovic, F. How membrane-active peptides get into lipid membranes. *Acc. Chem. Res.* **2016**, *49*, 1130−1138.

(7) Hong, J.; Lu, X.; Deng, Z.; Xiao, S.; Yuan, B.; Yang, K. How melittin inserts into cell membrane: conformational changes, inter-peptide cooperation, and disturbance on the membrane. *Molecules* **2019**, *24*, No. 1775.

(8) Beaugrand, M.; Arnold, A. A.; Hénin, J.; Warschawski, D. E.; Williamson, P. T.; Marcotte, I. Lipid concentration and molar ratio boundaries for the use of isotropic bicelles. *Langmuir* **2014**, *30*, 6162−6170.

(9) Warschawski, D. E.; Arnold, A. A.; Beaugrand, M.; Gravel, A.; Chartrand; Marcotte, I. Choosing membrane mimetics for NMR structural studies of transmembrane proteins. *Biochim. Biophys. Acta, Biomembr.* **2011**, *1808*, 1957−1974.

(10) Booth, V.; Warschawski, D. E.; Santisteban, N. P.; Laadhari, M.; Marcotte, I. Recent progress on the application of 2H solid-state NMR to probe the interaction of antimicrobial peptides with intact bacteria. *Biochim. Biophys. Acta, Biomembr.* **2017**, *1865*, 1500−1511.

(11) Kumar, K.; Arnold, A. A.; Gauthier, R.; Mamone, M.; Paquin, J.-F.; Warschawski, D. E.; Marcotte, I. 19F solid-state NMR approaches to probe antimicrobial peptide interactions with membranes in whole cells. *Biochim. Biophys. Acta, Biomembr.* **2024**, *1866*, No. 184269.

(12) Kumar, K.; Sebastiao, M.; Arnold, A. A.; Bourgault, S.; Warschawski, D. E.; Marcotte, I. In situ solid-state NMR study of antimicrobial peptide interactions with erythrocyte membranes. *Biophys. J.* **2022**, *121*, 1512−1524.

(13) Tardy-Laporte, C.; Arnold, A. A.; Genard, B.; Gastineau, R.; Morançais, M.; Mouget, J.-L.; Tremblay, R.; Marcotte, I. A 2H solid-state NMR study of the effect of antimicrobial agents on intact *Escherichia coli* without mutating. *Biochim. Biophys. Acta, Biomembr.* **2013**, *1828*, 614−622.

(14) Wimley, W. C. Describing the mechanism of antimicrobial peptide action with the interfacial activity model. *ACS Chem. Biol.* **2010**, *5*, 905−917.

(15) Melo, M. N.; Ferre, R.; Castanho, M. A. R. B. Antimicrobial peptides: linking partition, activity and high membrane-bound concentrations. *Nat. Rev. Microbiol.* **2009**, *7*, 245−250.

(16) Laadhari, M.; Arnold, A. A.; Gravel, A. E.; Separovic, F.; Marcotte, I. Interaction of the antimicrobial peptides caerin 1.1 and aurein 1.2 with intact bacteria by 2H solid-state NMR. *Biochim. Biophys. Acta, Biomembr.* **2016**, *1858*, 2959−2964.

(17) Malanovic, N.; Lohner, K. Antimicrobial peptides targeting gram-positive bacteria. *Pharmaceuticals* **2016**, *9*, No. 59.

(18) Ntallis, C.; Martin, N. I.; Edwards, A. M.; Weingarth, M. Bacterial cell envelope-targeting antibiotics. *Nat. Rev. Microbiol.* **2025**, 1−14.
(19) Marcotte, I.; Wegener, K. L.; Lam, Y.-H.; Chia, B. C.; de Planque, M. R.; Bowie, J. H.; Auger, M.; Separovic, F. Interaction of antimicrobial peptides from Australian amphibians with lipid membranes. *Chem. Phys. Lipids* **2003**, *122*, 107−120.
(20) Cardon, S.; Sachon, E.; Carlier, L.; Drujon, T.; Walrant, A.; Alemán-Navarro, E.; Martínez-Osorio, V.; Guianvarc'H, D.; Sagan, S.; Fleury, Y.; Marquant, R.; Piesse, C.; Rosenstein, Y.; Auvynet, C.; Lacombe, C. Peptidoglycan potentiates the membrane disrupting effect of the carboxyamidated form of DMS-DA6, a Gram-positive selective antimicrobial peptide isolated from Pachymedusa dacnicolor skin. *PLoS One* **2018**, *13*, No. e0205727.
(21) Fernandez, D. I.; Le Brun, A. P.; Whitwell, T. C.; Sani, M.-A.; James, M.; Separovic, F. The antimicrobial peptide aurein 1.2 disrupts model membranes via the carpet mechanism. *Phys. Chem. Chem. Phys.* **2012**, *14*, 15739−15751.
(22) Fernandez, D. I.; Sani, M.-A.; Miles, A. J.; Wallace, B. A.; Separovic, F. Membrane defects enhance the interaction of antimicrobial peptides, aurein 1.2 versus caerin 1.1. *Biochim. Biophys. Acta, Biomembr.* **2013**, *1828*, 1863−1872.
(23) Zaatouf, L.; Drujon, T.; Walrant, A.; Sachon, E.; Warschawski, D. E. Antimicrobial peptide mechanism of action on *S. aureus* membranes determined by in vivo solid-state NMR. *Biophys. Chem.* **2026**, *328*, No. 107532.
(24) Fernandez, D. I.; Gehman, J. D.; Separovic, F. Membrane interactions of antimicrobial peptides from Australian frogs. *Biochim. Biophys. Acta, Biomembr.* **2009**, *1788*, 1630−1638.
(25) Hayhurst, E. J.; Kailas, L.; Hobbs, J. K.; Foster, S. J. Cell wall peptidoglycan architecture in *Bacillus subtilis*. *Proc. Natl. Acad. Sci. U.S.A.* **2008**, *105*, 14603−14608.
(26) Vollmer, W.; Blanot, D.; De Pedro, M. A. Peptidoglycan structure and architecture. *FEMS Microbiol. Rev.* **2008**, *32*, 149−167.
(27) Bui, N. K.; Eberhardt, A.; Vollmer, D.; Kern, T.; Bougault, C.; Tomasz, A.; Simorre, J.-P.; Vollmer, W. Isolation and analysis of cell wall components from Streptococcus pneumoniae. *Anal. Biochem.* **2012**, *421*, 657−666.
(28) Kho, K.; Meredith, T. C. Extraction and Analysis of Bacterial Teichoic Acids. *Bio Protoc* **2018**, *8*, e3078.
(29) Kelly, J. E.; Chrissian, C.; Stark, R. E. Tailoring NMR experiments for structural characterization of amorphous biological solids: A practical guide. *Solid State Nucl. Magn. Reson.* **2020**, *109*, No. 101686.
(30) Kern, T.; Giffard, M.; Hediger, S.; Amoroso, A.; Giustini, C.; Bui, N. K.; Joris, B.; Bougault, C.; Vollmer, W.; Simorre, J.-P. Dynamics characterization of fully hydrated bacterial cell walls by solid-state NMR: evidence for cooperative binding of metal ions. *J. Am. Chem. Soc.* **2010**, *132*, 10911−10919.
(31) Bougault, C.; Ayala, I.; Vollmer, W.; Simorre, J.-P.; Schanda, P. Studying intact bacterial peptidoglycan by proton-detected NMR spectroscopy at 100 kHz MAS frequency. *J. Struct. Biol.* **2019**, *206*, 66−72.
(32) Miles, A. J.; Ramalli, S. G.; Wallace, B. DichroWeb, a website for calculating protein secondary structure from circular dichroism spectroscopic data. *Protein Sci.* **2022**, *31*, 37−46.
(33) Romaniuk, J. A. H.; Cegelski, L. Bacterial cell wall composition and the influence of antibiotics by cell-wall and whole-cell NMR. *Philos. Trans. R. Soc., B* **2015**, *370*, No. 20150024.
(34) Ghassemi, N.; Poulhazan, A.; Deligey, F.; Mentink-Vigier, F.; Marcotte, I.; Wang, T. Solid-state NMR investigations of extracellular matrixes and cell walls of algae, bacteria, fungi, and plants. *Chem. Rev.* **2022**, *122*, 10036−10086.
(35) Neuhaus, F. C.; Baddiley, J. A continuum of anionic charge: structures and functions of D-alanyl-teichoic acids in gram-positive bacteria. *Microbiol. Mol. Biol. Rev.* **2003**, *67*, 686−723.
(36) Kern, T.; Hediger, S.; Muller, P.; Giustini, C.; Joris, B.; Bougault, C.; Vollmer, W.; Simorre, J.-P. Toward the characterization of peptidoglycan structure and protein- peptidoglycan interactions by solid-state NMR spectroscopy. *J. Am. Chem. Soc.* **2008**, *130*, 5618−5619.
(37) Caudill, E. R.; Hernandez, R. T.; Johnson, K. P.; O'Rourke, J. T.; Zhu, L.; Haynes, C. L.; Feng, Z. V.; Pedersen, J. A. Wall teichoic acids govern cationic gold nanoparticle interaction with Gram-positive bacterial cell walls. *Chem. Sci.* **2020**, *11*, 4106−4118.
(38) Kim, S. J.; Chang, J.; Singh, M. Peptidoglycan architecture of Gram-positive bacteria by solid-state NMR. *Biochimica et Biophysica Acta (BBA)-Biomembranes* **2015**, *1848*, 350−362.
(39) Dyson, H. J.; Wright, P. E. Unfolded proteins and protein folding studied by NMR. *Chem. Rev.* **2004**, *104*, 3607−3622.
(40) Kelly, S. M.; Jess, T. J.; Price, N. C. How to study proteins by circular dichroism. *Biochim. Biophys. Acta, Biomembr.* **2005**, *1751*, 119−139.
(41) Bucki, R.; Janmey, P. A. Interaction of the gelsolin-derived antibacterial PBP 10 peptide with lipid bilayers and cell membranes. *Antimicrob. Agents Chemother.* **2006**, *50*, 2932−2940.
(42) Juhaniewicz-Debinska, J.; Dziubak, D.; Sek, S. Does the electrical double layer contribute to the mechanism of action of antimicrobial peptides? *ChemElectroChem* **2024**, *11*, No. e202400153.
(43) Koprivnjak, T.; Weidenmaier, C.; Peschel, A.; Weiss, J. P. Wall teichoic acid deficiency in *Staphylococcus aureus* confers selective resistance to mammalian group IIA phospholipase A2 and human -defensin 3. *Infect. Immun.* **2008**, *76*, 2169−2176.
(44) Saxena, D.; Maitra, R.; Bormon, R.; Czekanska, M.; Meiers, J.; Titz, A.; Verma, S.; Chopra, S. Tackling the outer membrane: facilitating compound entry into Gram-negative bacterial pathogens. *npj Antimicrob. Resist.* **2023**, *1*, No. 17.
(45) Hancock, R. E. W.; Chapple, D. S. Peptide antibiotics. *Antimicrob. Agents Chemother.* **1999**, *43*, 1317−1323.
(46) Peschel, A.; Vuong, C.; Otto, M.; Gotz, F. The D-alanine residues of *Staphylococcus aureus* teichoic acids alter the susceptibility to vancomycin and the activity of autolytic enzymes. *Antimicrob. Agents Chemother.* **2000**, *44*, 2845−2847.
(47) Collins, L. V.; Kristian, S. A.; Weidenmaier, C.; Faigle, M.; Van Kessel, K. P.; Van Strijp, J. A.; Götz, F.; Neumeister, B.; Peschel, A. *Staphylococcus aureus* strains lacking D-alanine modifications of teichoic acids are highly susceptible to human neutrophil killing and are virulence attenuated in mice. *J. Infect. Dis.* **2002**, *186*, 214−219.

https://doi.org/10.1021/jacs.5c18971
J. Am. Chem. Soc. 2026, 148, 7240−7250

SUPPORTING INFORMATION

Wall Teichoic Acids Are Direct Molecular Targets of Antimicrobial Peptides in Gram-Positive Bacteria

Arunima Sandeep[1], Laila Zaatouf[2], Alexandre A. Arnold[1], Dror E. Warschawski[1,2] & Isabelle Marcotte[*1]

[1]Department of Chemistry, Université du Québec à Montréal, Montréal, Québec H2X 2J6, Canada
[2]Chimie Physique et Chimie du Vivant, CPCV, CNRS UMR 8228, Sorbonne Université, École normale supérieure, PSL Université, 75005, Paris, France

*Corresponding Author :
Email : marcotte.isabelle@uqam.ca
Department of Chemistry
Université du Québec à Montréal

TABLE OF CONTENTS

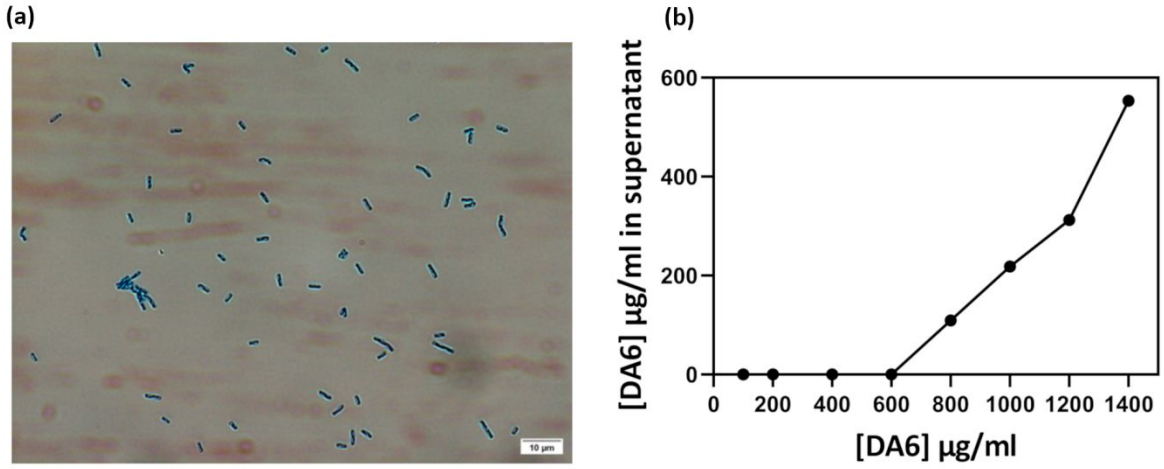

Figure S1: (a) Optical microscopy of extracted peptidoglycan from *B. subtilis* stained with crystal violet and imaged using a 60× oil immersion objective, showing that the shape of the *Bacillus* is retained after extraction. Scale bar: 10 µm. **(b)** Absorbance at 280 nm of the supernatant following incubation of PGN (1000 µg/mL) with DA6 shows complete binding below 600 µg/mL, justifying the use of a 1:2 (DA6:cell wall) mass ratio for ssNMR experiments.

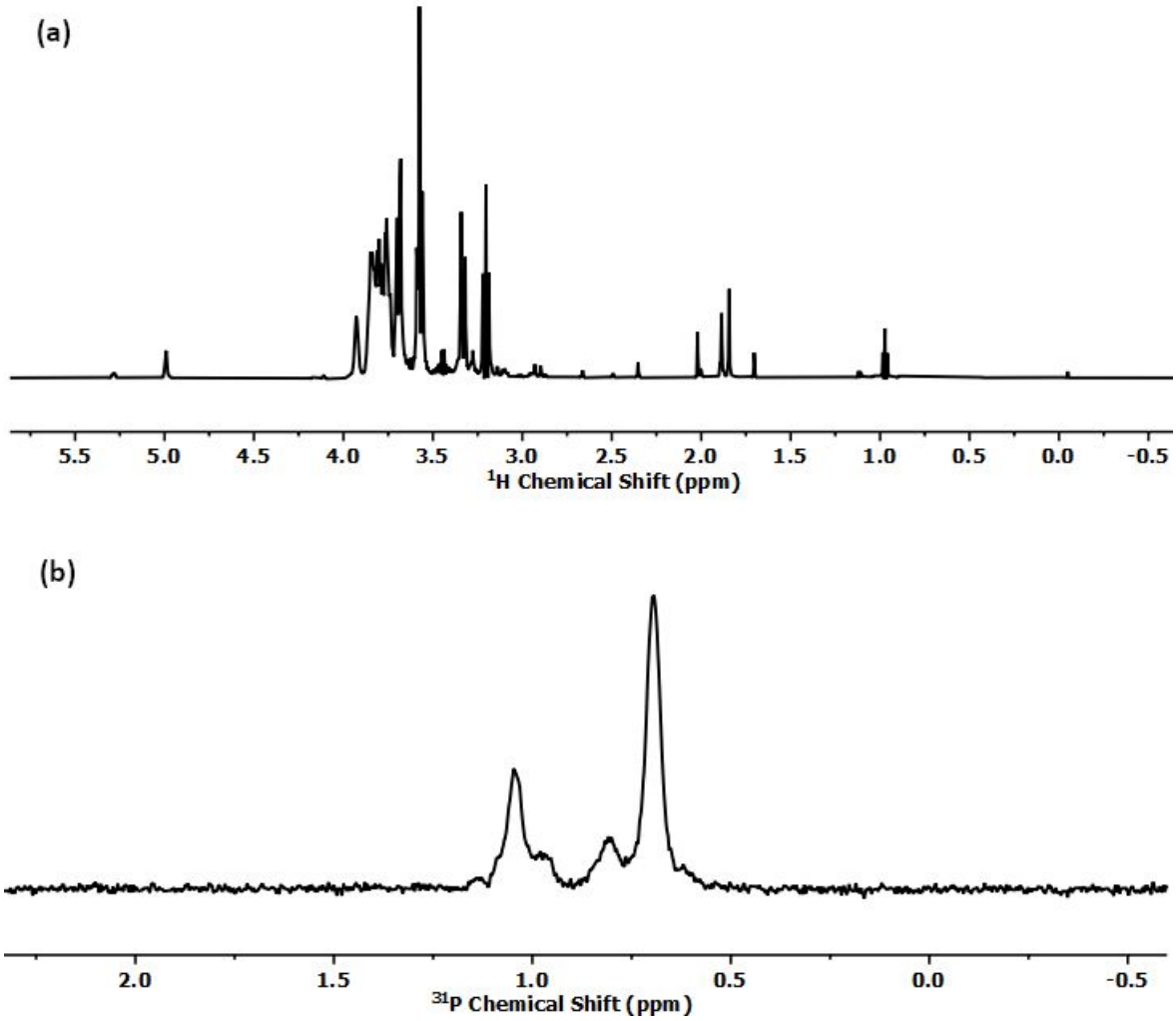

Figure S2: Solution NMR spectra of WTAs extracted by alkaline hydrolysis. Spectra were recorded at 600 MHz for samples at a concentration of 4 mg mL^{-1} in D_2O: (a) ^{1}H NMR spectrum acquired using water suppression with excitation sculpting and (b) ^{31}P NMR spectrum acquired using a direct-pulse experiment.

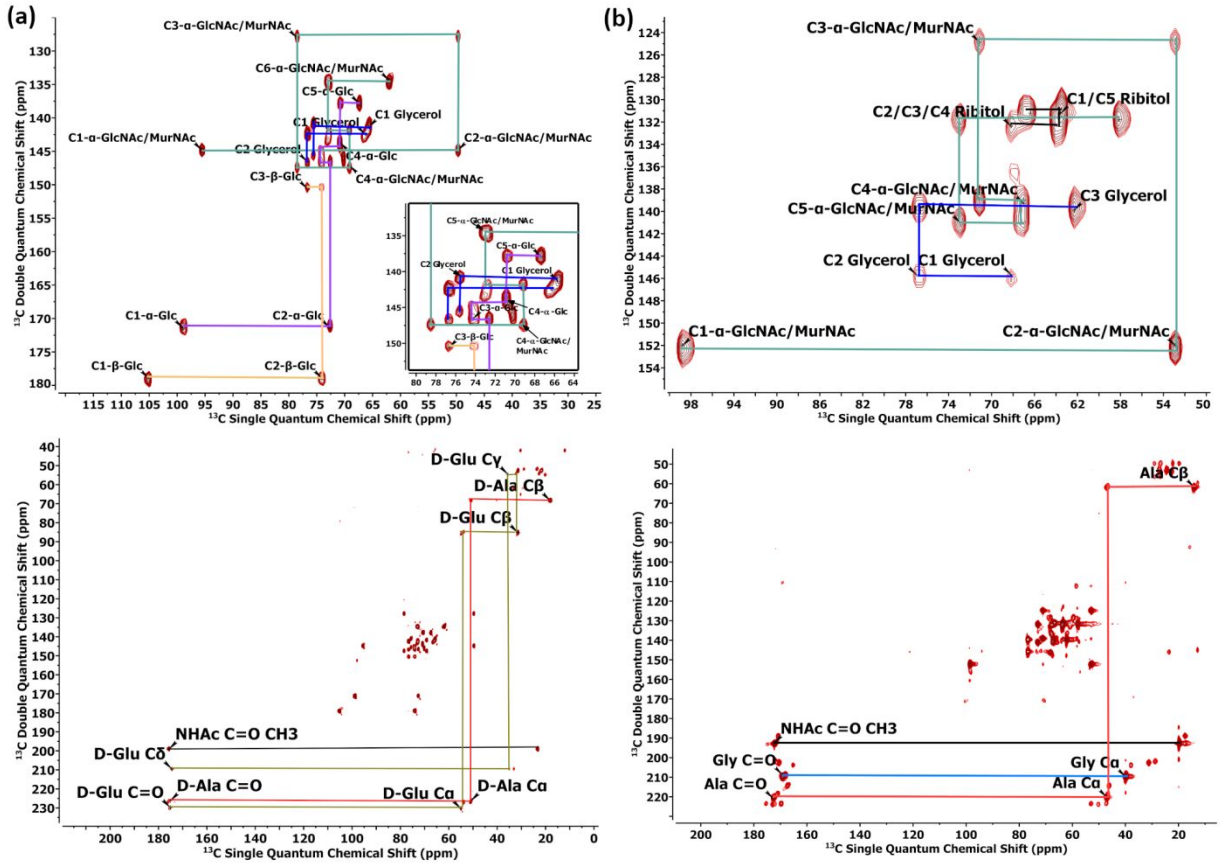

Figure S3: ^{13}C SQ-DQ RINADEQUATE assignment of the carbohydrate region (top) and peptide region (bottom) of **(a)** *B. subtilis* and **(b)** *S. aureus.* Spectra were recorded at 600 MHz using MAS at 15 kHz at a temperature of 15^{0}C. (Chemical shift values are detailed in Tables S1 and S2.)

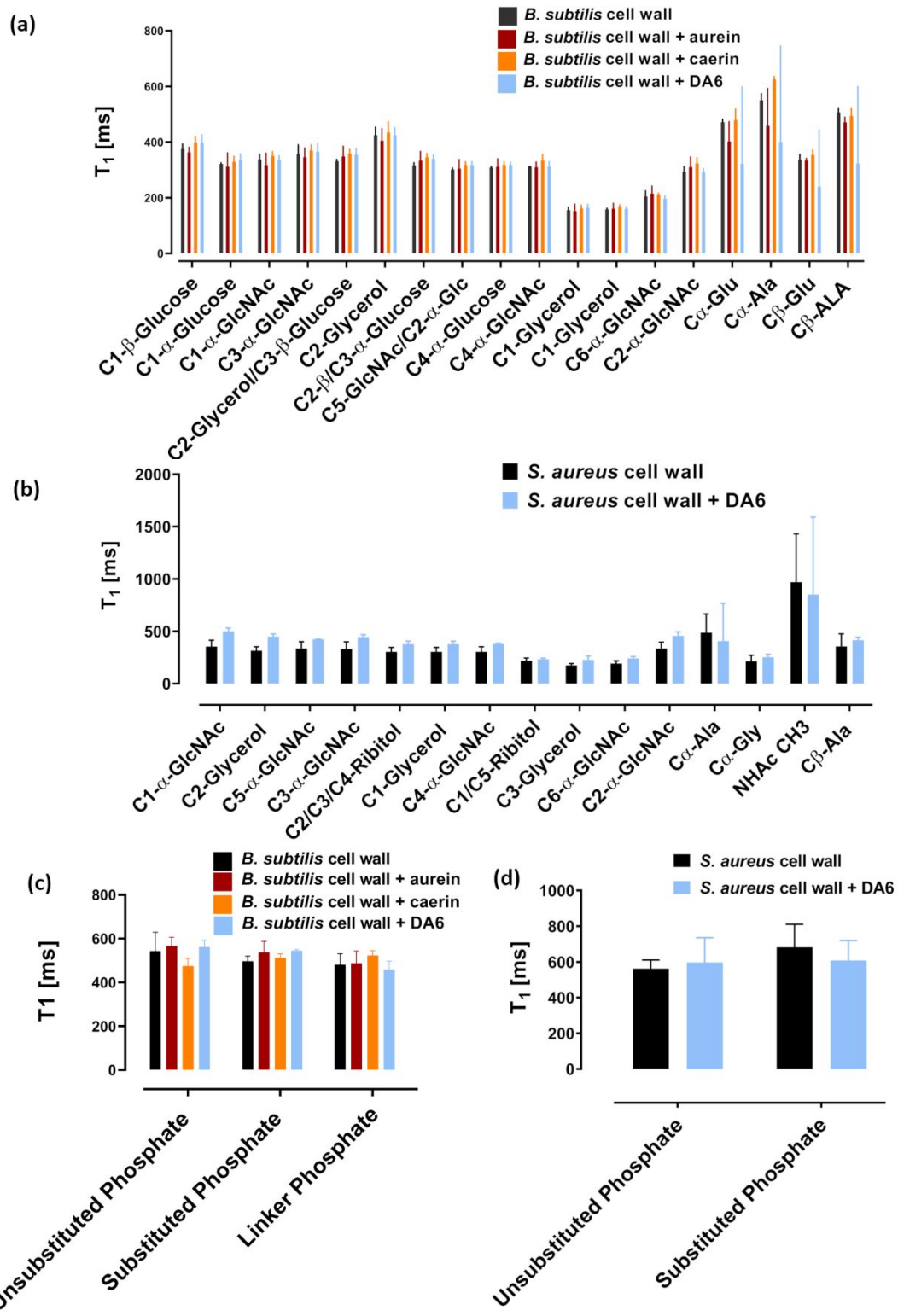

Figure S4: Effect of three cAMPs on the ^{13}C T_1 relaxation times in **(a)** *B. subtilis* and **(b)** of DA6 in *S. aureus*. **(c)** Effect of the cAMPs on the ^{31}P T_1 relaxation time in *B. subtilis* and in **(d)** *S. aureus,* showing no change in relaxation time.

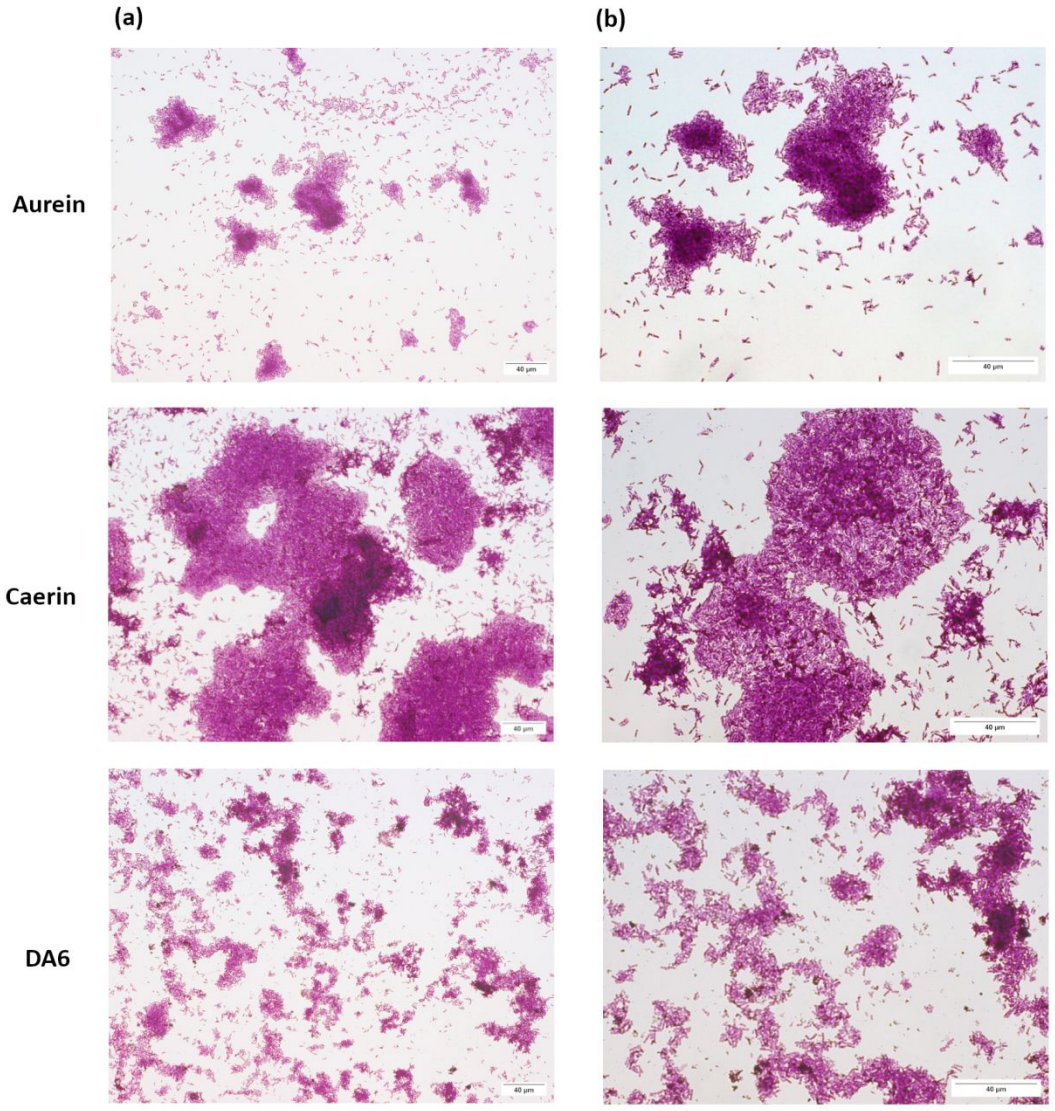

Figure S5: Crystal violet-stained cell wall microscopy images of *B. subtilis* in the presence of the three cAMPs (imaged after ssNMR experiment) at **(a)** 20× and **(b)** 40× magnification. Scale bars: 40 μm.

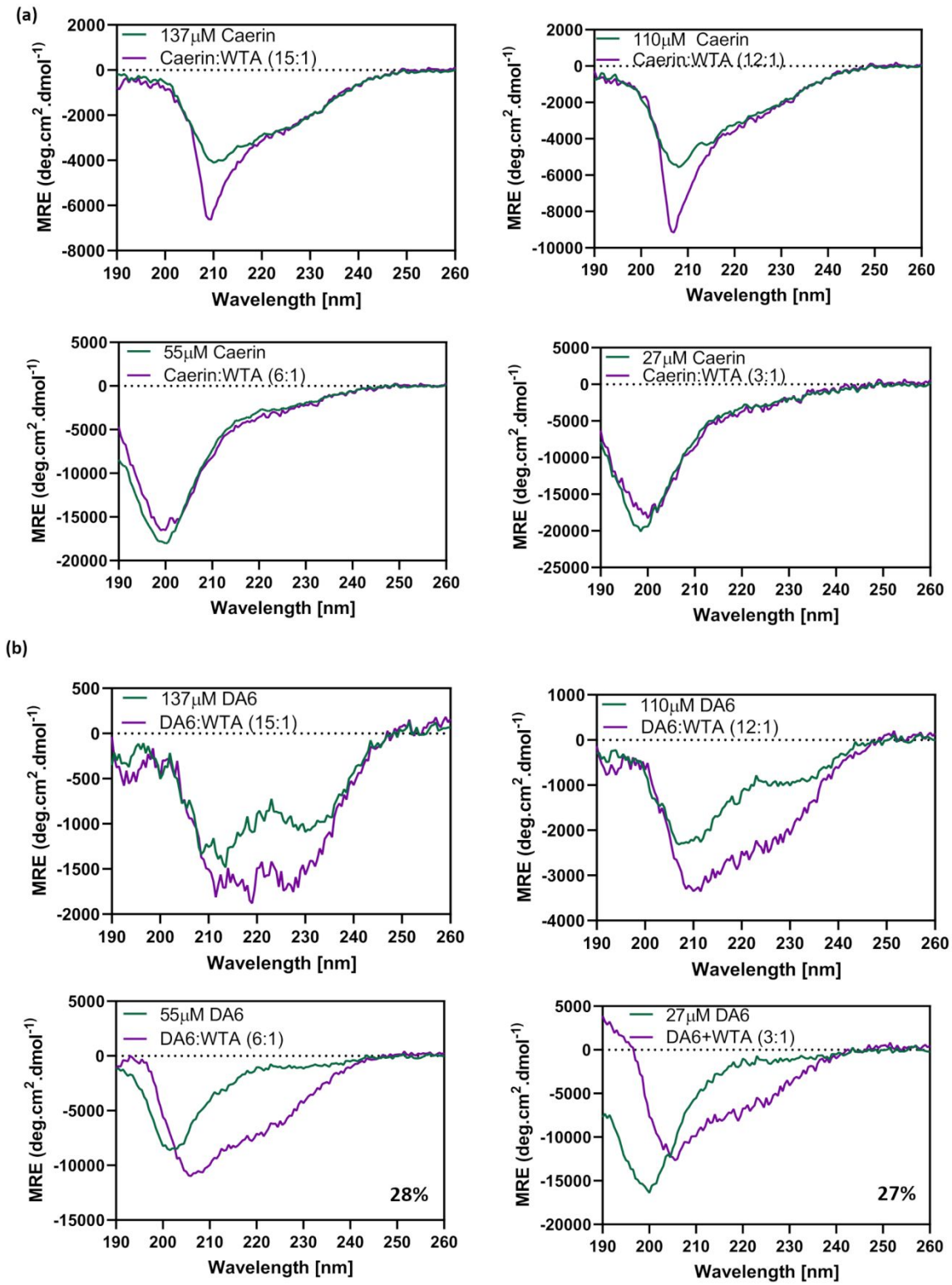

Figure S6: Conformation analysis of **(a)** caerin and **(b)** DA6 in the presence of WTA isolated from *B. subtilis* at various peptide-to-WTA molar ratios using CD spectroscopy at room temperature. The helicity value for DA6 is indicated in the figure.

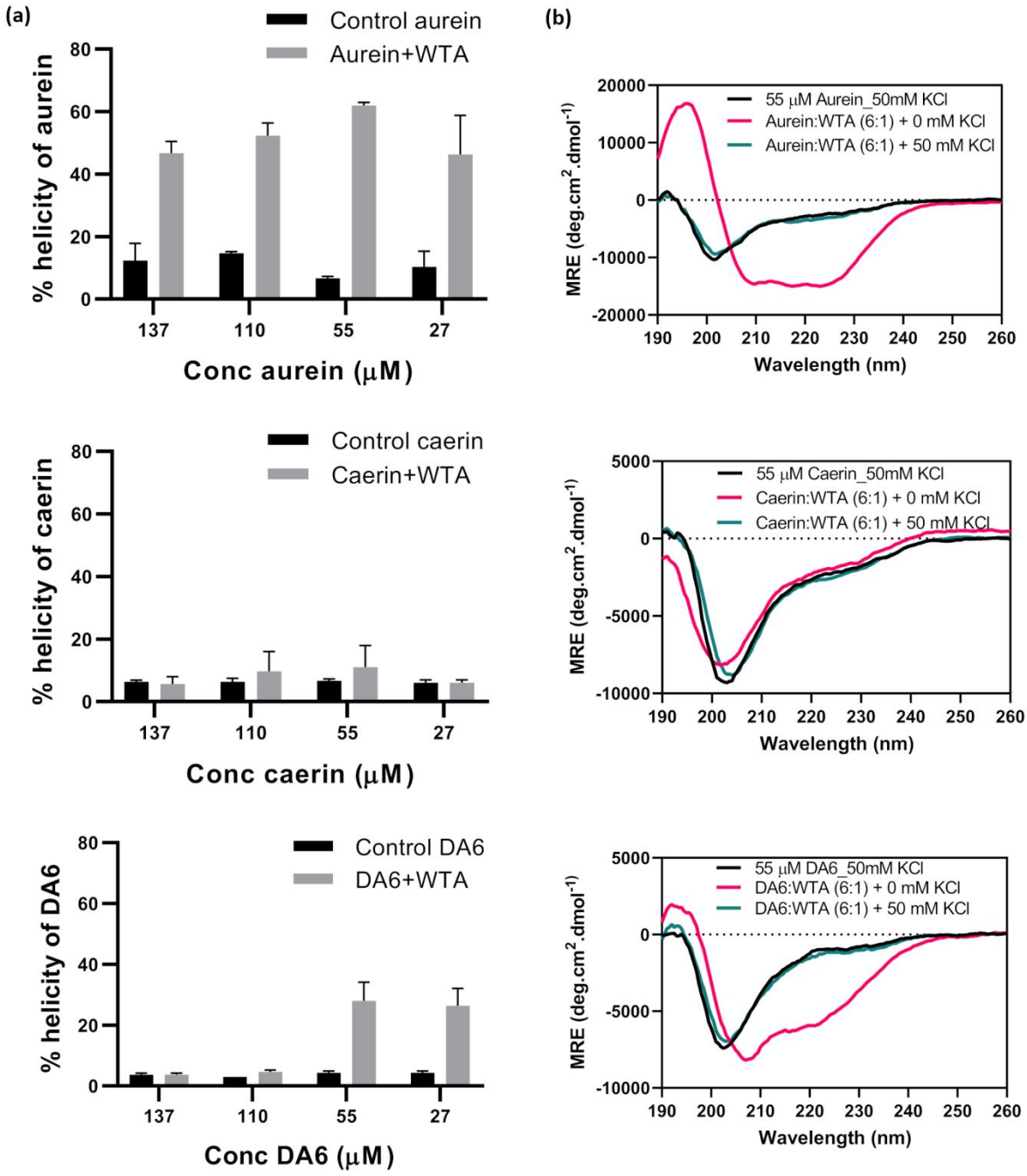

Figure S7: **(a)** Percent helicity of aurein, caerin, and DA6 in the absence and presence of wall teichoic acids in a range of molar concentrations (top to bottom). **(b)** Effect of 50 mM KCl on the secondary structure of aurein, caerin, and DA6 (top to bottom).

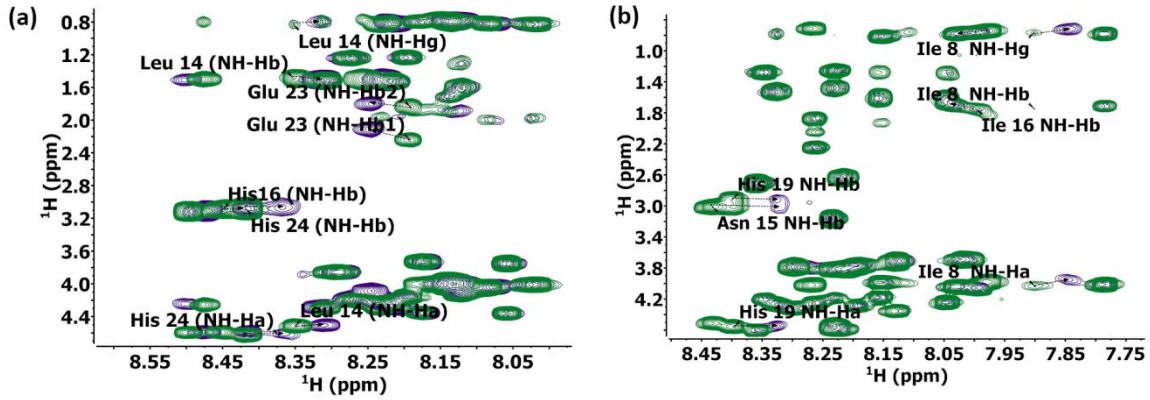

Figure S8: Overlayed ^{1}H-^{1}H TOCSY spectra highlighting the amide–aliphatic correlations of peptides with and without WTA at 15:1 (peptide:WTA) molar ratio. Spectra show the peptide alone in green and with WTA in purple for **(a)** caerin, and **(b)** DA6 under identical experimental conditions (23°C, 600 MHz). Key cross-peaks corresponding to residue-specific interactions are indicated and all the residues are elaborated in Tables S3-S5.

Table S1: Carbon resonance assignment in the cell wall of *B. subtilis*.[1] (*Empty rows correspond to positions where no assignment could be made. *D- and L-alanine residues could not be distinguished. Diaminopimelic acid in the peptidoglycan was not assigned.)

Molecule	Atoms	Experimental (ppm)	Kern et al.[2] & BMRB (ppm)
α-GlcNAc/ MurNAc	C1	95.59	95.1
	C2	49.68	49.5
	C3	78.53	78.2
	C4	69.1	69
	C5	72.64	72.7
	C6	62.04	61.4
	NHAc CO	175.84	175.2
	NHAc CH_3	23.34	23
α-Glc	C1	98.99	98.5
	C2	72.65	72.5
	C3	74.22	74
	C4	70.88	70.7
	C5	67.38	72.9
	C6		61.4
β-Glc	C1	105.12	105
	C2	74.09	73.8
	C3	76.69	
	C4	*	
	C5		
	C6		
Glycerol	C1	65.66 and 66.27	66.1
	C2	75.6 and 76.7	76.2
	C3		65.4
D/L-Ala*	C=O	175.13	177.75
	Cα	50.86	53.15
	Cβ	18	19.03
D-Glu	C=O	175.15	176.84
	Cα	54.98	57.32
	Cβ	31.43	29,99
	Cδ	174.48	181.21
	Cγ	35.52	36.14

Table S2: Carbon resonance assignment in the cell wall of *S. aureus*. (*Empty rows correspond to positions where no assignment could be made. *Variations in chemical shifts might be due to the different strains used in this work (strain ATCC 6538) and the reference (strain RN4220). Lys and Glu of PGN were not assigned.)

Molecule	Atoms	Experimental (ppm)	Xia, Guoqing et al.*[3] & BMRB (ppm)
α-GlcNAc/ MurNAc	C1	98.79	97.61
	C2	52.89	55.08
	C3	71.13	72.22
	C4	67.01	71.39
	C5	72.9	72.22
	C6	58.18	61.85
	NHAc CO	172.26	
	NHAc CH_3	19	
Glycerol	C1	68.19	66.1
	C2	77.02	76.2
	C3	62.3	65.4
Ribitol	C1	63.48	67.92
	C2	68.19 and 66.42	71.31
	C3	68.19 and 66.42	71.3
	C4	68.19 and 66.42	78.83
	C5	63.48	65.72
D-Ala	C=O	172.75	177.75
	Cα	47.01	53.15
	Cβ	14.03	19.03
Gly	C=O	169.26	173
	Cα	39.9	45

Table S3: ^{1}H chemical shift assignment obtained from the TOCSY experiments performed on aurein in the absence and presence of *B. subtilis'* wall teichoic acid at various molar ratios prepared in nanopure water.

	Annotation	NH Aur	NH Aur+ WTA (12:1)	NH Aur+ WTA (15:1)	NH Aur+ WTA (30:1)	Ha/Hb Aur	Ha/Hb Aur+ WTA (12:1)	Ha/Hb Aur+ WTA (15:1)	Ha/Hb Aur+ WTA (30:1)
1	Leu 2 NH- Ha	8.42	8.46	8.46	8.44	4.13	4.04	4.04	4.07
2	Leu 2 NH- Hb	8.42	8.46	8.46	8.45	1.32	1.27	1.28	1.3
3	Leu 2 NH- Hd	8.42	8.44	8.46	8.45	0.74	0.68	0.7	0.73
4	Phe3 NH- Ha	8.23	8.24	8.25	8.24	4.54	4.59	4.57	4.56
5	Phe 3 NH- Hb1	8.23	8.24	8.25	8.24	2.89	2.85	2.85	2.86
6	Phe 3 NH- Hb2	8.23	8.25	8.25	8.24	3.08	3.18	3.17	3.14
7	Asp 4 NH-Ha	8.11	7.82	7.84	7.92	4.52	4.46	4.46	4.48
8	Asp 4 NH-Hb	8.12	7.82	7.84	7.92	2.63	2.53	2.53	2.56
9	Ile 5 NH-Ha	7.95	7.95	7.95	7.95	4	4	4	4
10	Ile 5 NH-Hb	7.95	7.95	7.95	7.95	1.76	1.79	1.78	1.76
11	Ile 5 NH-Hg	7.95	7.95	7.95	7.95	0.78	0.78	0.79	0.78
12	Ile 6 NH-Ha	8.06	8.05	8.05	8.05	3.99	3.98	4	3.99
13	Ile 6 NH-Hb	8.06	8.05	8.05	8.05	1.76	1.76	1.78	1.76
14	Ile 6 NH-Hg	8.06	8.05	8.05	8.05	0.77	0.78	0.78	0.78
15	Lys 7 NH-Ha	8.23	8.23	8.24	8.23	4.18	4.15	4.17	4.17
16	Lys 7 NH-Hb	8.23	8.23	8.23	8.2	1.61	1.61	1.61	1.63
17	Lys 7 NH-Hd	8.23	8.24	8.25	8.2	1.28	1.28	1.28	1.29
18	Lys 8 NH-Ha	8.2	8.19	8.18	8.2	4.19	4.17	4.19	4.19
19	Lys 8 NH-Hb	8.2	8.19	8.2	8.17	1.64	1.63	1.64	1.66
20	Lys 8 NH-Hd	8.2	8.18	8.19	8.17	1.28	1.28	1.31	1.3
21	Ile 9 NH-Ha	8.1	8.1	8.1	8.09	4	4	4	4.02
22	Ile 9 NH-Hb	8.09	8.1	8.1	8.09	1.74	1.75	1.75	1.74
23	Ile 9 NH-Hg	8.09	8.1	8.1	8.09	0.8	0.8	0.8	0.8
24	Ala 10 NH- Ha	8.28	8.28	8.28	8.26	4.19	4.19	4.19	4.19
25	Ala 10 NH- Hb	8.28	8.28	8.28	8.25	1.27	1.27	1.27	1.27
26	Glu 11 NH-Ha	8.18	8.18	8.22	8.18	4.2	4.2	4.15	4.18
27	Glu 11 NH-Hb	8.17	8.23	8.22	8.18	2.28	2.16	2.19	2.26
28	Glu 11 NH-Hg	8.17	8.23	8.22	8.18	1.84	1.82	1.83	1.84
29	Ser 12 NH-Ha	8.14	8.11	8.12	8.12	4.28	4.28	4.28	4.28
30	Ser 12 NH-Hb	8.14	8.11	8.12	8.12	3.67	3.68	3.67	3.67
31	Phe 13 NH- Hb1	8.11	8.07	8.08	8.09	2.9	2.91	2.91	2.91
32	Phe 13 NH- Hb2	8.11	8.07	8.08	8.09	3.09	3.11	3.09	3.1

Table S4: ^{1}H chemical shift assignment obtained from the TOCSY experiments performed on caerin in the absence and presence of *B. subtilis'* wall teichoic acid at various molar ratios prepared in nanopure water.

	Annotation	NH Cae	NH Cae+ WTA (12:1)	NH Cae+ WTA (15:1)	NH Cae+ WTA (30:1)	Ha/Hb Cae	Ha/Hb Cae+ WTA (12:1)	Ha/Hb Cae+ WTA (15:1)	Ha/Hb Cae+ WTA (30:1)
1	Leu 2 (NH-Ha)	8.31	8.32	8.31	8.31	4.3	4.28	4.3	4.3
2	Leu 2 (NH-Hb)	8.31	8.31	8.31	8.31	1.52	1.52	1.52	1.52
3	Leu 2 (NH-Hg)	8.31	8.31	8.32	8.31	0.79	0.79	0.8	0.79
4	Leu 3 (NH-Ha)	8.48	8.5	8.49	8.48	4.26	4.24	4.24	4.26
5	Leu 3 (NH-Hb)	8.48	8.5	8.49	8.48	1.5	1.49	1.5	1.5
6	Leu 3 (NH-Hg)	8.48	8.5	8.49	8.48	0.8	0.8	0.79	0.8
7	Ser 4 (NH-Ha)	8.17	8.17	8.17	8.18	4.35	4.35	4.35	4.35
8	Ser 4 (NH-Hb)	8.18	8.17	8.17	8.18	3.75	3.74	3.74	3.72
9	Val 5 (NH-Ha)	8.09	8.08	8.08	8.09	4.05	4.04	4.04	4.05
10	Val 5 (NH-Hb)	8.09	8.07	8.08	8.09	2	2	2.01	2
11	Val 5 (NH-Hg)	8.09	8.07	8.07	8.09	0.82	0.82	0.82	0.82
12	Leu 6 (NH-Hb)	8.21	8.22	8.22	8.21	1.54	1.53	1.52	1.54
13	Leu 6 (Nh-Ha)	8.22	8.21	8.22	8.22	4.24	4.23	4.24	4.24
14	Gly 7 (NH-Ha)	8.29	8.29	8.29	8.29	3.86	3.86	3.86	3.86
15	Ser 8 (NH-Ha)	8.06	8.05	8.05	8.06	4.37	4.37	4.35	4.37
16	Ser 8 (NH-Hb)	8.06	8.05	8.05	8.06	3.75	3.75	3.75	3.75
17	Ala 10 (NH-Ha)	8.27	8.27	8.27	8.26	4.22	4.19	4.19	4.21
18	Ala 10 (NH-Hb)	8.27	8.27	8.27	8.27	1.24	1.24	1.24	1.24
19	Lys 11 (NH-Hg)	8.12	8.12	8.12	8.12	1.3	1.31	1.31	1.3
20	Lys 11 (NH-Ha)	8.13	8.13	8.13	8.13	4.12	4.14	4.12	4.12
21	Lys 11 (NH-Hd)	8.12	8.12	8.12	8.12	1.6	1.61	1.61	1.6
22	Lys 11 (NH-He)	8.12	8.12	8.11	8.12	2.87	2.87	2.86	2.87
23	His 12 (NH-Ha)	8.5	8.46	8.48	8.49	4.6	4.58	4.59	4.6
24	His 12 (NH-Hb)	8.5	8.47	8.48	8.49	3.12	3.1	3.11	3.12
25	Val 13 (NH-Ha)	8.15	8.12	8.13	8.15	4	4	4	4
26	Val 13 (NH-Hb)	8.15	8.12	8.13	8.15	1.89	1.9	1.89	1.89
27	Val 13 (NH-Hg)	8.14	8.12	8.13	8.14	0.79	0.79	0.79	0.79
28	Leu 14 (NH-Ha)	8.35	8.3	8.31	8.34	4.52	4.5	4.5	4.5
29	Leu 14 (NH-Hb)	8.35	8.38	8.36	8.34	1.49	1.63	1.53	1.49
30	Leu 14 (NH-Hg)	8.35	8.38	8.37	8.34	0.83	0.87	0.83	0.83
31	His 16 (NH-Ha)	8.45	8.41	8.42	8.45	4.59	4.58	4.59	4.59
32	His 16 (NH-Hb)	8.45	8.41	8.42	8.45	3.09	3.06	3.08	3.09
33	Val 18 (NH-Hg)	8.17	8.17	8.17	8.17	0.79	0.79	0.79	0.79
34	Ala 22 (NH-Ha)	8.19	8.19	8.19	8.21	4.16	4.16	4.16	4.15
35	Ala 22 (NH-Hb)	8.2	8.2	8.2	8.2	1.23	1.23	1.23	1.23
36	Glu 23 (NH-Hb1)	8.19	8.25	8.24	8.21	2.26	2.11	2.12	2.19
37	Glu 23 (NH-Hb2)	8.19	8.25	8.24	8.21	1.84	1.79	1.8	1.82
38	His 24 (NH-Ha)	8.42	8.35	8.38	8.41	4.63	4.61	4.61	4.63
39	His 24 (NH-Hb)	8.42	8.36	8.38	8.41	3.08	3.08	3.06	3.08
40	Leu 25 (NH-Hb)	8.26	8.26	8.26	8.25	1.51	1.51	1.51	1.49
41	Val 9/ Ile 21(NH-	8.02	8.02	8.02	8.02	4.01	4.01	4.01	4.01
42	Val 9/ Ile 21(NH-Hb)	8.02	8.02	8.02	8.02	1.98	1.98	1.98	1.98
43	Val 9/ Ile 21(NH-Hg)	8.02	8.02	8.02	8.02	0.83	0.83	0.83	0.83
44	Val 17/ 20 (NH-Ha)	8.23	8.23	8.23	8.23	4.28	4.28	4.28	4.28
45	Val 17/ 20 (NH-Hb)	8.23	8.2	8.21	8.23	1.95	1.95	1.96	1.95
46	Val 17/ 20 (NH-Hg)	8.23	8.21	8.21	8.23	0.83	0.83	0.83	0.83

Table S5: ^{1}H chemical shift assignment obtained from the TOCSY experiments performed on DA6 in the absence and presence of *B. subtilis'* wall teichoic acid at various molar ratios prepared in nanopure water.

	Annotation	NH DA6	NH DA6+ WTA (12:1)	NH DA6+ WTA (15:1)	NH DA6+ WTA (30:1)	Ha/Hb DA6	Ha/Hb DA6+ WTA (12:1)	Ha/Hb DA6+ WTA (15:1)	Ha/Hb DA6+ WTA (30:1)
1	Gly 1 NH-Ha	7.95	7.95	7.95	7.95	3.7	3.72	3.72	3.72
2	Val 2 NH-Ha	8.1	8.11	8.11	8.11	3.97	4	4	4
3	Val 2 NH-Hb	8.1	8.1	8.1	8.1	1.85	1.86	1.86	1.86
4	Val 2 NH-Hg	8.1	8.11	8.11	8.11	0.73	0.75	0.75	0.75
5	Trp 3 NH-Ha	8.26	8.26	8.26	8.26	4.25	4.26	4.26	4.26
6	Trp 3 NH-Hb1	8.26	8.26	8.26	8.26	1.86	1.86	1.87	1.87
7	Trp 3 NH-Hb2	8.26	8.26	8.26	8.26	2.25	2.24	2.24	2.24
8	Gly 4 NH-Ha	8.01	8.02	8.02	8.02	3.69	3.68	3.68	3.68
9	Ile 5 NH-Hb	7.78	7.78	7.78	7.78	1.71	1.71	1.71	1.71
10	Ile 5 NH-Hg	7.78	7.79	7.79	7.79	0.78	0.78	0.78	0.78
11	Ile 5 NH-Ha	7.78	7.78	7.78	7.78	4.02	4.01	4.01	4.01
12	Ala 6 NH-Ha	8.34	8.34	8.34	8.34	4.18	4.21	4.21	4.21
13	Ala 6 NH-Hb	8.34	8.34	8.34	8.35	1.28	1.28	1.28	1.28
14	Lys 7 NH-Ha	8.22	8.23	8.23	8.23	4.18	4.19	4.19	4.19
15	Lys 7 NH-Hb1	8.22	8.23	8.23	8.23	1.25	1.26	1.26	1.26
16	Lys 7 NH-Hb2	8.22	8.23	8.23	8.23	1.48	1.47	1.47	1.47
17	Ile 8 NH-Ha	7.9	7.85	7.89	7.92	4.03	3.93	3.96	3.97
18	Ile 8 NH-Hb	7.9	7.84	7.88	7.92	1.74	1.79	1.85	1.83
19	Ile 8 NH-Hg	7.9	7.85	7.89	7.92	0.76	0.72	0.72	0.74
20	Ala 9 NH-Ha	8.04	8.04	8.04	8.04	4.24	4.24	4.24	4.24
21	Ala 9 NH-Hb	8.04	8.04	8.04	8.04	1.28	1.3	1.3	1.3
22	Gly 10 NH-Ha	8.21	8.21	8.21	8.21	3.82	3.82	3.82	3.82
23	Lys 11 NH-Ha	7.95	7.94	7.94	7.95	4.21	4.22	4.2	4.19
24	Lys 11 NH-Hb1	7.95	7.93	7.95	7.95	1.23	1.23	1.31	1.24
25	Lys 11 NH-Hb2	7.95	7.95	7.94	7.95	1.45	1.37	1.46	1.46
26	Val 12 NH-Ha	8.03	8.03	8.03	8.03	4.04	4.04	4.04	4.04
27	Val 12 NH-Hb	8.03	8.04	8.04	8.04	1.67	1.65	1.68	1.65
28	Val 12 NH-Hg	8.02	8.02	8.02	8.02	0.78	0.78	0.78	0.78
29	Leu 13 NH-Ha	8.26	8.27	8.27	8.27	4.02	4.03	4.03	4.03
30	Leu 13 NH-Hd	8.26	8.27	8.27	8.27	0.71	0.71	0.75	0.71
31	Gly 14 NH-Ha1	8.07	8.09	8.09	8.09	4.34	4.35	4.35	4.35
32	Gly 14 NH-Ha2	8.07	8.08	8.08	8.08	3.78	3.72	3.72	3.72
33	Asn 15 NH-Ha	8.43	8.29	8.43	8.43	4.5	4.52	4.5	4.5
34	Asn 15 NH-Hb	8.43	8.29	8.32	8.35	3.01	2.97	3	2.99
35	Ile 16 NH-Ha	7.97	7.99	7.99	8	3.99	4.07	4.07	4.06
36	Ile 16 NH-Hb	7.99	7.99	7.99	7.99	1.76	1.75	1.75	1.75
37	Ile 16 NH-Hg	7.98	7.99	7.99	8	0.74	0.76	0.76	0.76
38	Leu 17 NH-Ha	8.32	8.33	8.33	8.33	4.26	4.27	4.27	4.27
39	Leu 17 NH-Hb	8.32	8.33	8.33	8.33	1.54	1.53	1.53	1.53
40	Leu 17 NH-Hd	8.32	8.32	8.32	8.32	0.8	0.78	0.78	0.78
41	His 19 NH-Ha	8.4	8.33	8.4	8.4	4.56	4.55	4.56	4.56
42	His 19 NH-Hb	8.4	8.33	8.35	8.37	2.91	2.9	2.92	2.89
43	Val 20 NH-Ha	8.15	8.15	8.15	8.15	3.98	3.98	3.98	3.98
44	Val 20 NH-Hb	8.14	8.16	8.16	8.15	1.93	1.9	1.94	1.93
45	Val 20 NH-Hg	8.14	8.15	8.15	8.15	0.81	0.82	0.82	0.82
46	Phe 21 NH-Ha	8.22	8.23	8.23	8.23	4.56	4.56	4.57	4.57
47	Phe 21 NH-Hb1	8.23	8.23	8.23	8.23	3.17	3.18	3.16	3.16
48	Phe 21 NH-Hb2	8.21	8.21	8.21	8.21	2.63	2.63	2.64	2.64
49	Ser 22 NH-Ha	8.13	8.12	8.12	8.12	3.71	3.71	3.71	3.72
50	Ser 22 NH-Hb	8.13	8.12	8.12	8.12	4.36	4.35	4.35	4.35
51	Ser 23 NH-Ha	8.29	8.3	8.3	8.29	4.32	4.32	4.32	4.32
52	Ser 23 NH-Hb	8.29	8.28	8.28	8.29	3.78	3.78	3.79	3.79
53	Asn 24 NH-Ha	8.35	8.36	8.35	8.36	4.61	4.61	4.57	4.61
54	Asn 24 NH-Hb	8.35	8.35	8.35	8.36	2.7	2.71	2.71	2.71
55	Gln 25 NH-Ha	8.15	8.15	8.15	8.15	4.18	4.17	4.17	4.17
56	Gln 25 NH-Hb1	8.15	8.15	8.15	8.15	1.28	1.28	1.28	1.28
57	Gln 25 NH-Hb2	8.15	8.15	8.15	8.15	1.61	1.61	1.61	1.61
58	Ser 26 NH-Ha	8.19	8.19	8.19	8.19	4.29	4.29	4.29	4.29
59	Ser 26 NH-Hb	8.19	8.19	8.19	8.19	3.78	3.79	3.78	3.78

Table S6: Composition for the preparation of 1× M9 in 1 L:

Component	Amount	Concentration
Sodium Phosphate Dibasic Heptahydrate ($Na_2HPO_4.7H_2O$) (Mw:268.07 g/mol)	12.8 g	0.04774 M
Potassium Phosphate Monobasic (KH_2PO_4) (MW:136.09 g/mol)	3.0 g	0.02204 M
Sodium Chloride (NaCl) (MW:58.44 g/mol)	0.5 g	0.00855 M
Ammonium Chloride (NH_4Cl) (MW:53.49 g/mol)	**1.0 g**	**0.01869 M**
Magnesium Sulphate ($MgSO_4$) (MW:120.36 g/mol)	120.0 mg	1.00000 mM
Calcium Chloride ($CaCl_2$) (MW:110.98 g/mol)	11.0 mg	0.10000 mM

Table S7: Carbon source and vitamin for M9 media preparation in 300 mL.

Component	Amount	Concentration
Glucose ($C_6H_{12}O_6$) (MW: 180.16 g/mol)	**1g**	**3.3 mg/mL**
Biotin (MW: 244.31 g/mol)	3mg	10 µg/mL
Thiamine (MW: 265.35 g/mol)	3mg	10 µg/mL

Table S8: Composition for the preparation of trace element solution (10 mL of trace element mix for 1 L of culture)

Element	Mass per 100 mL
$FeSO_4.7H_2O$	0.60 g
$MnCl_2.4H_2O$	0.12 g
$CoCl_2.6H_2O$	0.08 g
$ZnSO_4.7H_2O$	0.07 g
$CuCl_2.2H_2O$	0.03 g
H_3BO_3	2 mg
$(NH_4)_6Mo_7O_{24}.4H_2O$	0.025 g
EDTA	0.50 g

PROTOCOLS

(S1) MIC determination

1) Prepare an overnight culture of the bacteria.
2) Next morning transfer 300µL of the overnight culture to 30mL of media and let it grow to mid-exponential phase.
3) Prepare a 96 well-sterile plate and add 100µL of media to each of the required wells.
4) Prepare a stock of the peptide to be tested at 256µg/mL.
5) Serially dilute the peptide in the wells by adding 100µL in the first well then mixing and transferring 100µL to the next well, so on and so forth.
6) Once the bacteria have reached the mid exponential phase prepare a stock of the bacteria at 0.006 OD and add 100µL of this to each well to reach a final starting OD of 0.003 for Gram(+) bacteria.
7) Leave the prepared plates in the incubator at 37^0C overnight with shaking at 150rpm.
8) The well with zero growth for the lowest concentration of the peptide is taken as the MIC.

(S2) ^{13}C/^{15}N labeling of *B. subtilis* & *S. aureus*

1) First prepare **M9 media** as per table S6.
2) Adjust pH to 7.2 and then autoclave.
3) To make 300mL culture measure 280mL of M9 to 3 L Erlenmeyer flask.
4) Make the **carbon source and vitamin** solution in table S7 in 10mL nano pure water.
5) Using sterile filter (0.22 µm) transfer the 10mL glucose and 3mL of **trace element solution** (table S8) to the M9 media.
6) Finally, from the overnight preculture add bacteria to start at an OD of 0.1.
7) The culture takes around 16hr to grow (Early stationary phase)

-In the case of ^{13}C labelling, glucose is replaced by ^{13}C-glucose;
-In the case of ^{15}N labelling, ammonium chloride is replaced by ^{15}N-ammonium chloride.

(S3) Cell wall extraction

1) 0.1M Tris buffer with pH 6.8 is used in the procedure.
2) Start by keeping water to boil (90-100 °C) inside the hood. Keep a smaller vessel around 50mL within the 500mL vessel to hold the glass tubes and the thermometer.
3) Make solution of 1% SDS (200mg in 20mL).
4) Pour 5mL of 1% SDS to four glass tubes and keep it for heating (1min).
5) The bacteria recovered by centrifugation at 3000g for 10 min (4°C) and then freeze dried is mixed with buffer. Equal volumes of bacteria are transferred to the SDS solutions.
6) Cover the tubes with aluminium foil and poke a few holes to let out steam. Boil at 100 °C for 30 min.
7) Allow it to cool to room temperature. Do not use ice or the SDS will precipitate. Transfer to 50mL tube.

8) Centrifuge at 4000g for 10 min. Wash with nanopure water until the solution no longer forms.
9) Resuspend pellet in nano pure water (20mL) and put in sonication bath for 30 minutes.
10) Centrifuge at 4000g for 15 min, then dissolve in solution containing 0.1 M Tris pH 7.5 (20mL) and 100 µg/mL (2mg in 20mL) of α-amylase. Incubate 2hr at 37 °C.
11) Centrifuge at 4000g for 15 min. Add solution containing 0.1 M Tris pH 6.8, 20mM $MgSO_4$ (48.1mg in 20mL), 15 µg/mL DNase (0.3mg in 20mL), and 60 µg/mL RNase (1.2 mg in 20mL). Incubate for 2hr at 37 °C.
12) Centrifuge at 4000g for 15 min. Resuspend pellet in a solution with 10 mM $CaCl_2.2H_2O$ (29.4 mg in 20 mL) and 100 µg/mL Trypsin (2mg in 20 mL). Incubate 16hr at 37 °C.
13) Deactivate enzymes with 1% SDS. Boil for 15 min.
14) Centrifuge at 4000g for 15 min. Wash with 8 M LiCl (6.8g in 20mL water). Next wash with 100mM EDTA (0.6g in 20mL water) to chelate the metals and remove them. Wash twice with water and once with acetone.
15) Resuspend in 5mL water to lyophilise.
16) Rehydrate and transfer sample to rotor.
17) The extraction yields around 18-22 weight% cell wall from lyophilised bacteria.

REFERENCES

(1) Bougault, C.; Ayala, I.; Vollmer, W.; Simorre, J.-P.; Schanda, P. Studying intact bacterial peptidoglycan by proton-detected NMR spectroscopy at 100 kHz MAS frequency. *Journal of structural biology* **2019**, *206* (1), 66-72.
(2) Kern, T.; Giffard, M.; Hediger, S.; Amoroso, A.; Giustini, C.; Bui, N. K.; Joris, B.; Bougault, C.; Vollmer, W.; Simorre, J.-P. Dynamics characterization of fully hydrated bacterial cell walls by solid-state NMR: evidence for cooperative binding of metal ions. *Journal of the American Chemical Society* **2010**, *132* (31), 10911-10919.
(3) Xia, G.; Maier, L.; Sanchez-Carballo, P.; Li, M.; Otto, M.; Holst, O.; Peschel, A. Glycosylation of wall teichoic acid in Staphylococcus aureus by TarM. *Journal of Biological Chemistry* **2010**, *285* (18), 13405-13415.